

The Population of Weak Mg II Absorbers I. A Survey of 26 QSO HIRES/Keck Spectra^{1,2}

Christopher W. Churchill³, Jane R. Rigby, Jane C. Charlton⁴

*Department of Astronomy and Astrophysics
The Pennsylvania State University, University Park PA 16802
cwc, jrigby, charlton@astro.psu.edu*

and

Steven S. Vogt^{3,5}

*Board of Astronomy and Astrophysics
University of California, Santa Cruz CA 95064
vogt@ucolick.org*

ABSTRACT

We present a search for “weak” MgII absorbers [those with $W_r(2796) < 0.3 \text{ \AA}$] in the HIRES/Keck spectra of 26 QSOs. We found 30, of which 23 are newly discovered. The spectra are 80% complete to $W_r(2796) = 0.02 \text{ \AA}$ and have a cumulative redshift path of ~ 17.2 for the redshift range $0.4 \leq z \leq 1.4$. The number of absorbers per unit redshift, dN/dz , is seen to increase as the equivalent width threshold is decreased; we obtained $dN/dz = 1.74 \pm 0.10$ for our $0.02 \leq W_r(2796) < 0.3 \text{ \AA}$ sample. The equivalent width distribution follows a power law, $N(W) \propto W^{-\delta}$, with $\delta \sim 1.0$; there is no turnover down to $W_r(2796) = 0.02 \text{ \AA}$ at $\langle z \rangle = 0.9$. Weak absorbers comprise at least 65% of the total MgII absorption population, which outnumbers Lyman limit systems (LLS) by a factor of 3.8 ± 1.1 ; the majority of weak MgII absorbers must arise in sub-LLS environments. Tentatively, we predict that $\sim 5\%$ of the Ly α forest clouds with $W_r(\text{Ly}\alpha) \geq 0.1 \text{ \AA}$ will have detectable MgII absorption to $W_r^{\text{min}}(2796) = 0.02 \text{ \AA}$ and that this is primarily a high-metallicity selection effect ($[Z/Z_\odot] \geq -1$). This implies that MgII absorbing structures figure prominently as tracers of sub-LLS environments where gas has been processed by stars. We compare the number density of $W_r(2796) \geq 0.02 \text{ \AA}$ absorbers with that of both high and low surface brightness galaxies and find a fiducial absorber size of $35h^{-1}$ to $63h^{-1}$ kpc, depending upon the assumed galaxy population and their absorption properties. The individual absorbing “clouds” have $W_r(2796) \leq 0.15 \text{ \AA}$ and their narrow (often unresolved) line widths imply temperatures of $\sim 25,000$ K. We measured $W_r(1548)$ from CIV in FOS/HST archival spectra and, based upon comparisons with FeII, found a range of ionization conditions (low, high, and multi-phase) in absorbers selected by weak MgII.

¹Based in part on observations obtained at the W. M. Keck Observatory, which is jointly operated by the University of California and the California Institute of Technology.

²Based in part on observations obtained with the NASA/ESA *Hubble Space Telescope*, which is operated by the STScI for the Association of Universities for Research in Astronomy, Inc., under NASA contract NAS5-26555.

³Visiting Astronomer at the W. M. Keck Observatory

⁴Center for Gravitational Physics and Geometry, Pennsylvania State University

⁵UCO/Lick Observatories, University of California

1. Introduction

We present a survey for “weak” MgII $\lambda\lambda 2976, 2803$ absorption in the spectra of QSOs obtained with the HIRES spectrograph (Vogt et al. 1994) on the Keck I telescope. There have been several MgII surveys over the previous decade (Lanzetta, Turnshek, & Wolfe 1987, hereafter LTW; Tytler et al. 1987, hereafter TBSYK; Caulet 1989; Petitjean & Bergeron 1990, hereafter PB90; Sargent, Steidel, & Boksenberg 1988, hereafter SSB; Steidel & Sargent 1992, hereafter SS92). These surveys were complete to a rest-frame MgII $\lambda 2796$ equivalent width, $W_r(2796)$, of 0.3 \AA and above. The more comprehensive work of SS92 yielded solid statistics on the equivalent width distribution, redshift number density, large scale velocity clustering, and evolution over the redshift range $0.3 \leq z \leq 2.2$, for which the MgII doublet can be observed with ground based telescopes.

The shape of the $W_r(2796)$ distribution function at smaller equivalent widths has important implications for our understanding of cosmic chemical evolution and its connection to star producing environments. At $0.3 \leq z \leq 1.0$, MgII absorption with $W_r(2796) \geq 0.3 \text{ \AA}$ MgII has been found to arise within $\sim 40h^{-1} \text{ kpc}^6$ of normal galaxies (Bergeron & Boissé 1991; Steidel, Dickinson, & Persson 1994). These galaxies exhibit a wide range of colors from late-type spirals to the reddest ellipticals (though more luminous galaxies are redder), and have L_B and L_K luminosity functions consistent with the local luminosity function (types later than Sd are absent). It has been concluded that a wide range of morphological types are contributing to the MgII absorbing gas cross section, except that isolated low-mass ($L_K \leq 0.06L_K^*$) “faint blue galaxies” are not (Steidel, Dickinson, & Persson 1994). A rapid cut off in the equivalent width distribution would imply that this observed sample of galaxies provides a complete picture of the star forming environments that give rise to MgII absorbing gas. Currently, that picture is one in which the galaxy population selected by MgII absorption is stable, showing very little cosmological evolution from $z \sim 1$ (but see Lilly et al. 1995).

If, on the other hand, the number of MgII absorbers per unit redshift continues to rise for decreasing $W_r(2796)$, it would be implied that surveys complete to 0.3 \AA have unveiled only a small portion of the

population of metal-line systems selected by MgII absorption. Churchill & Le Brun (1998) have discussed this possibility based upon the discovery of two near-solar to super-solar metallicity MgII absorbers in the Ly α forest of PKS 0454 + 039. As such, our current picture of the relationship between MgII absorbing gas and star forming environments may require some modification. Perhaps the observed $L_K \sim 0.06L_K^*$ cut off in the luminosity function of MgII absorption-selected galaxies or the cut off at $\sim 40h^{-1} \text{ kpc}$ of MgII absorption around these galaxies does not apply for $W_r(2796) < 0.3 \text{ \AA}$. Alternatively, perhaps another population of star forming objects that preferentially give rise to weaker MgII absorption is implied. Or, perhaps both a slight modification to the current picture of MgII absorbing galaxies *and* the incorporation of another population of objects would be implied. Measuring the statistical absorption properties of the weakest MgII absorbers is a first step toward verifying or casting new light on such speculations.

For $W_r(2796) < 0.3 \text{ \AA}$, PB90 and SS92 inferred a cut off in the MgII equivalent width distribution, the number of absorbers per unit redshift per unit equivalent width. However, the completeness of their data below 0.3 \AA dropped rapidly. Their conclusions have necessarily been based upon a comparison of the number of MgII absorbers detected with $W_r(2796) < 0.3 \text{ \AA}$, corrected for completeness, to the number of these absorbers *predicted* by extrapolating the equivalent width distribution. Measurements of the equivalent width distribution, however, were somewhat inconclusive; the data were adequately described either by a power law distribution with slope $\delta = 2.0$ (TBSYK) or $\delta = 1.6$ (SS92), or by an exponential with a characteristic equivalent width of $W_r(2796) = 0.66 \text{ \AA}$ (SS92; LTW). Womble (1995) and Tripp, Lu, & Savage (1997) have tentatively concluded that the equivalent width distribution continues to rise below 0.3 \AA .

The HIRES/Keck spectra obtained for the thesis of Churchill (1997a) provide duplicate redshift coverage of 26 of the 103 QSO sight lines studied by SS92. The spectra are 80% complete to $W_r^{\min}(2796) = 0.02 \text{ \AA}$, and provide an opportunity to directly investigate if in fact there is a paucity of MgII absorbers with $W_r(2796) < 0.3 \text{ \AA}$ and to measure the shape of the distribution of equivalent widths well below 0.3 \AA . Archival FOS spectra from the *Hubble Space Telescope (HST)* cover the CIV $\lambda\lambda 1548, 1550$ doublet, which is a useful indicator of the ionization condi-

⁶Throughout this paper we use $q_0 = 0.05$ and express physical sizes in terms of $h = H_0/100$.

tions. For systems with redshifts greater than ~ 1.2 , ground-based spectra (taken from the literature) cover CIV.

The acquisition of the data and their reduction and analysis are described in §2. In §3, we present our adopted sample of weak MgII systems. In §4 we compute the redshift path density, determine the shape of the equivalent width distribution, examine the clustering, and discuss the general absorption properties of weak MgII absorbers. We present the results from a FOS/*HST* survey and literature search for associated CIV and discuss the ionization conditions and constraints on the absorption cross sections in §5. Our main results are summarized in §6.

2. Observations and Data Analysis

2.1. The Sample of QSO Spectra

A full description of the HIRES data acquisition is given in Churchill (1997a) and in Churchill, Vogt, & Charlton (1998, hereafter CVC98). In short, 26 QSO spectra were obtained with the HIRES spectrometer (Vogt et al. 1994) on the Keck I telescope. The QSOs and their emission redshifts, the UT date of the observations, the summed exposure times, and the approximate wavelength coverage are presented in Table 1. The spectra comprise a biased sample of QSO sight lines with “strong” MgII absorbers. However, the QSO lines of sight are unbiased for MgII systems with $W_r(2796) < 0.3 \text{ \AA}$, since nothing is known *a priori* about the presence of these “weak” MgII systems⁷. It is possible that weak systems are preferentially found in sight lines along which strong systems are present, in which case these QSO spectra would not comprise an unbiased sample. We return to this point in §4.3. Because of the echelle format, each spectrum has breaks in wavelength coverage redward of 5100 Å. The gaps in redshift coverage begin at $z \sim 0.83$ and become more pronounced toward higher redshifts (see Figure 1a). The FOS/*HST* data have either been collected from the *HST* archive (in collaboration with S. Kirhakos, B. Jannuzi, and D. Schneider) or are from the QSO Absorption Line Key Project (Bahcall et al. 1996; Jannuzi et al. 1998).

⁷From this point forward, we refer to “weak” systems as those having $W_r(2796) < 0.3 \text{ \AA}$ and call $W_r(2796) \geq 0.3 \text{ \AA}$ systems “strong”.

2.2. The HIRES/Keck Data

The raw data frames were bias corrected, flat fielded, cosmic ray cleaned, combined, and scattered light corrected, using the standard IRAF⁸ packages following the techniques described in Churchill (1995). The individual spectra were extracted using the optimal extraction algorithms provided in the *Aextract* package. The wavelength calibration was done interactively using the *ecidentify* task of the *Echelle* package. We have not resampled the data by linearizing the wavelength as a function of pixel along the dispersion direction. The continuum fits, based upon the formalism of Sembach & Savage (1992), were obtained by minimizing χ^2 between the flux values and a smooth function, usually a Legendre polynomial. For the detection of weak unresolved features, it is critical that the measured uncertainty in each resolution element accurately reflects the continuum noise. Therefore, for each echelle order, we enforced a unity χ_ν^2 between the smooth fitted continuum model and the spectrum by scaling the uncertainty spectrum (output by *aextract*) by a single “optimizing” multiplicative factor, f . To obtain f , we root solved the function $1 - \chi_\nu^2$, where $\chi_\nu^2 = V_{\text{fit}}/fV_\sigma$, and V_{fit} and V_σ are the variance in the continuum fit and the uncertainty spectrum, respectively. The process required an automated iterative convergence algorithm in order to objectively mask absorption features from the fit.

For the objective identification of unresolved absorption (and emission) features, we have used the formalism presented by Schneider et al. (1993). The resulting equivalent width uncertainty spectra provide the observed equivalent width detection threshold as a function of wavelength. The 5σ rest-frame equivalent width limits of the $\lambda 2796$ transition are shown in Figure 1a as a function of redshift. Where there is no redshift coverage (interorder gaps), we have arbitrarily set the limiting equivalent width to zero.

Only a single exposure of Q0002+051 was obtained so that removing cosmic rays, especially from the sky, was problematic. As a consequence, the zero level of the spectrum is uncertain by $\sim 10\%$ and the measured equivalent widths may be biased by this probable zero-point offset, which varied from echelle order to echelle order. This uncertainty has not been included in the error estimate of the quoted equivalent

⁸IRAF is distributed by the National Optical Astronomy Observatories, which are operated by AURA, Inc., under contract to the National Science Foundation.

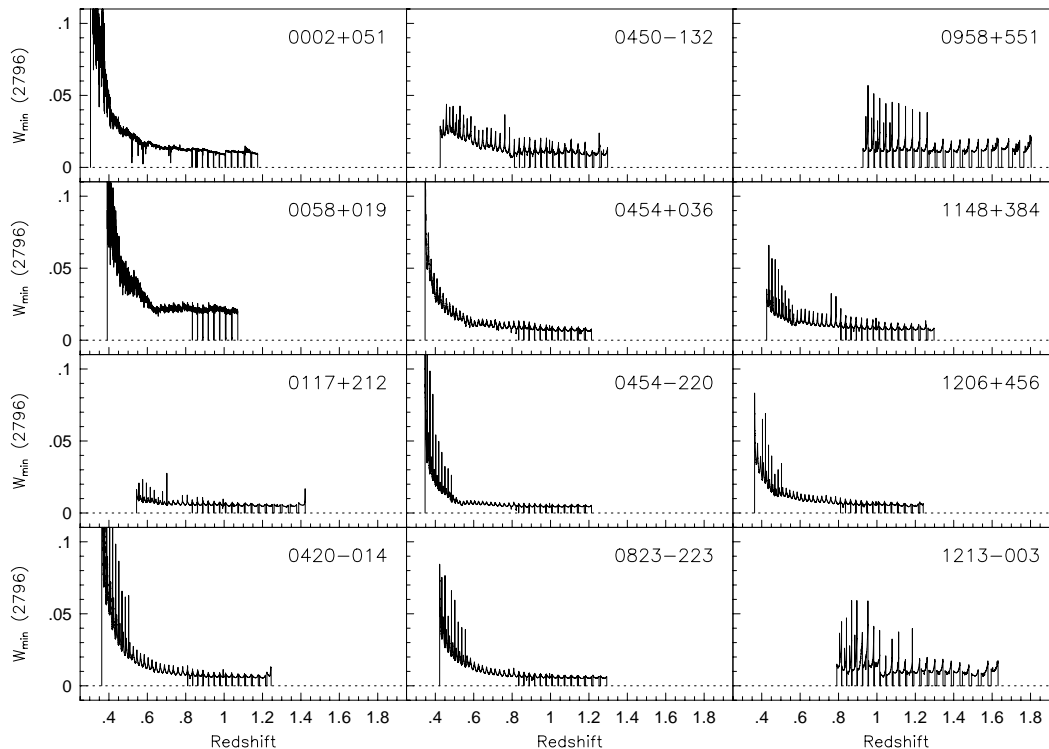


Fig. 1a.— The survey sensitivity, given as the $5\sigma W_r^{\min}(2796)$, is shown as a function of redshift. Breaks in the echelle spectral coverage, where there is no possibility of detecting a MgII doublet in a given redshift range, are arbitrarily assigned $W_r^{\min}(2796) = 0$.

widths. In Q1548 + 092, the Ly α forest compromises all transitions of metal line systems that lie blueward of $\sim 4560 \text{ \AA}$. Thus, we have not searched for MgII doublets in this spectrum below $z \sim 0.62$.

2.3. The FOS/*HST* data

We searched for CIV $\lambda\lambda 1548, 1550$ doublets at the redshifts of weak MgII absorbers in FOS/*HST* spectra. These spectra were originally collected together for a companion paper (Churchill et al. 1998, Paper II). The archival data have been retrieved and reduced in collaboration with S. Kirhakos, B. Jannuzi, and D. Schneider using the techniques and software of the *HST* QSO Absorption Line Key Project. The remaining spectra, which were originally obtained for the *HST* Key Project, have been kindly provided by our collaborators in fully reduced form. In Table 1, we reference the available spectra and the grating that covered CIV. For details of the data reduction see Schneider et al. (1993), Bahcall et al. (1996), and Jannuzi et al. (1998).

2.4. Doublet Searching

The search for MgII doublets involved the following steps. First, a complete list of 5σ features were ob-

jectively defined in each HIRES spectrum. To locate candidate MgII doublets, we then tested the features one by one, starting at the smallest wavelength feature and moving toward larger wavelengths. We assumed each feature was a candidate $\lambda 2796$ line with observed central wavelength λ_{27} . Then, the expected location of the $\lambda 2803$ feature was computed from $\lambda_{28} = 2803.531(\lambda_{27}/2796.352)$. Centered about λ_{28} , an equivalent width and its uncertainty were measured in an aperture with the same full width at the continuum as that of the candidate $\lambda 2796$ feature. These quantities were measured using the formalism of Sembach & Savage (1992). The pair was designated as a candidate doublet when the $\lambda 2803$ detection significance was roughly equal to or greater than half that of the $\lambda 2796$ feature (given by the ratio of the $f\lambda$) and when the doublet ratio was consistent with $1 \leq \text{DR} \leq 2$ within the 1σ uncertainties.

We also employed a quantitative measure of the chance that the candidate $\lambda 2803$ transition could be a random feature or a transition from another system⁹ along the QSO sight line. A “false alarm” prob-

⁹We have performed an exhaustive cross-checking of line identifications from CIV and MgII redshifts reported in the literature and from those discovered in our spectra. Details of the line

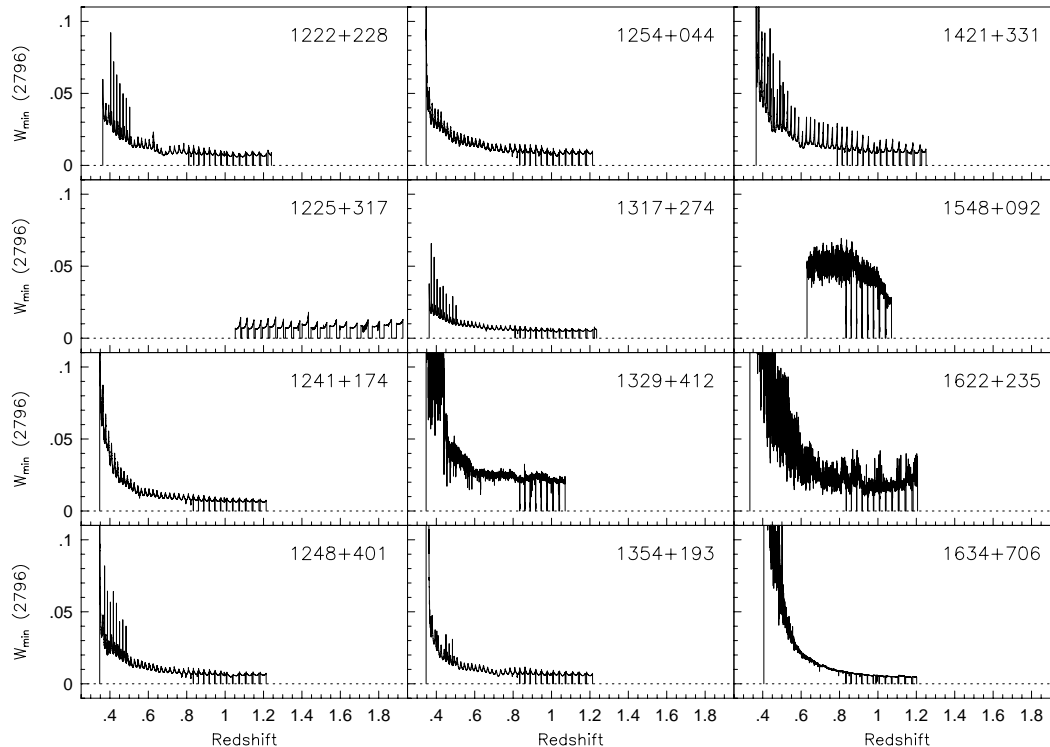


Fig. 1b.— Same as for figure 1a

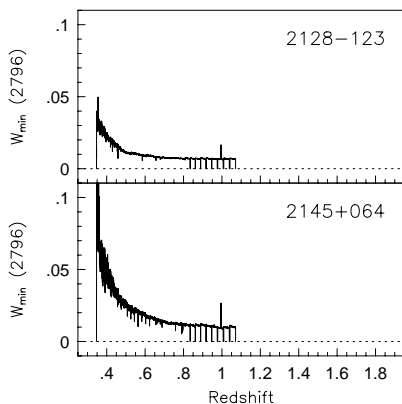


Fig. 1c.— Same as for figure 1a

ability is computed by scanning the spectrum pixel by pixel (also with an aperture given by the full width at the continuum of the candidate $\lambda 2796$ feature). The scan is performed about 50 \AA to both sides of the candidate $\lambda 2803$ feature. This corresponds to a to-

identifications and the list of searched transitions and redshifts will be presented in CVC98.

tal redshift window of $\Delta z \sim 0.02$, or $\pm 3000 \text{ km s}^{-1}$ about the feature. The false alarm probability is simply the fraction of pixels with detected features (both emission and absorption) having a significance level greater than or equal to the candidate $\lambda 2803$ feature. The detection levels of the $\lambda 2803$ transitions for all included doublets were greater than 4.5σ . Most bonafide MgII doublets have false alarm probabilities of $P_{\text{fa}} \leq 10^{-6}$. The largest false alarm probability, for S24 in Q1213 – 003 at $z = 1.1277$, was $P_{\text{fa}} \sim 0.009$. We are quite certain that our adopted sample is not contaminated by false MgII systems.

In addition to the above constraints, a nearest neighbor velocity separation of greater than 500 km s^{-1} was enforced. The velocity filter was applied so that small equivalent width, high velocity components in strong systems would not be included in the sample. The 500 km s^{-1} separation criterion resulted in our dropping only a single potential weak MgII absorber from our sample in Q1206 + 456 (see “system A” in Churchill & Charlton 1998).

The search for CIV in the FOS/*HST* spectra was performed in an identical fashion as the MgII doublets, except that the objective line list was relaxed to 3σ detections¹⁰. We visually inspected each spec-

¹⁰We acknowledge A. Dobrzycki, who kindly assisted us in a preliminary search for CIV doublets in the FOS/*HST* spectra of

trum to determine if a candidate CIV doublet (at the redshift of a weak MgII system) was real or a blend of Ly α lines. If real, we measured $W_r(1548)$ using the same techniques used for the HIRES data. If not, we measure the 3σ equivalent width limit. We verified our results with the literature, when possible, but all quoted CIV equivalent widths and limits are based upon our measurements in order to maintain uniformity.

3. The Doublet Sample

Our adopted sample includes 30 systems and is presented in Table 2. Tabulated are the system number, the absorption redshift, the QSO spectrum in which it was detected, the velocity width in km s^{-1} of the $\lambda 2796$ transition, the rest-frame equivalent width of the $\lambda 2796$ transition, and the MgII doublet ratio. The last column contains the cumulative redshift path, $Z(W_r, DR)$, which is the total redshift path over which the tabulated system could have been detected in this survey (see Eq. 2). The velocity widths, ω_v , are measured directly from the flux values according to

$$\omega_v^2 = \int_{v_-}^{v_+} \tau_a(v)(\Delta v)^2 dv / \int_{v_-}^{v_+} \tau_a(v) dv, \quad (1)$$

where $\tau_a(v) = \ln[I_c(v)/I(v)]$ is the apparent optical depth (Savage & Sembach 1991), $I_c(v)$ is the continuum flux at velocity v , $I(v)$ is the measured flux at v , $\Delta v = v - \langle v \rangle$, and $\langle v \rangle$ is the velocity centroid of the absorption profile. The ω_v are mathematically equivalent to the Gaussian width of a normal distribution.

In Table 3, we present the properties of each system, including the transition identity, the observed wavelength, and the rest-frame equivalent width or its 3σ upper limit. The equivalent widths and their uncertainties are computed using the methods of Sembach & Savage (1992). For all MgII systems, we searched the HIRES spectrum for other transitions with the significance level relaxed to 3σ . Because the FeII and MgI $\lambda 2853$ transitions are the strongest and most commonly found in MgII absorbers, we have presented their limits. Other transitions are included in Table 3 when they have been detected. The data are shown in Figure 2a. Features marked with a “*” are either members of other systems or are unidentified.

Dobrzycki et al. (1998)

3.1. Discussion of Systems

3.1.1. S1 (Q1421 + 331; $z_{\text{abs}} = 0.45642$)

There is no previous report of S1. No FeII transitions were captured by the CCD. MgI was not detected. A FOS/*HST* spectrum of this QSO was not available. There is no galaxy candidate (C. Steidel, private communication).

3.1.2. S2 (Q1329 + 412; $z_{\text{abs}} = 0.500786$)

S2 was reported as a “probable” MgII doublet by SSB. This system is associated with a blueish low mass galaxy with $\simeq 0.05L_K^*$ at an impact parameter of $\simeq 5h^{-1}$ kpc (C. Steidel, private communication). The signal-to-noise ratio of the HIRES spectrum is fairly low, and only the MgII doublet was detected. CIV was not detected in the FOS/*HST* spectrum.

3.1.3. S3 (Q1354 + 193; $z_{\text{abs}} = 0.52149$)

There is no previous report of S3. Though FeII and MgI were captured by the CCD, only the MgII doublet was detected. CIV was not detected in the FOS/*HST* spectrum (also see Jannuzi et al. 1998). This QSO field has about five galaxies at $z \sim 0.5$, which are part of a foreground cluster (C. Steidel, private communication).

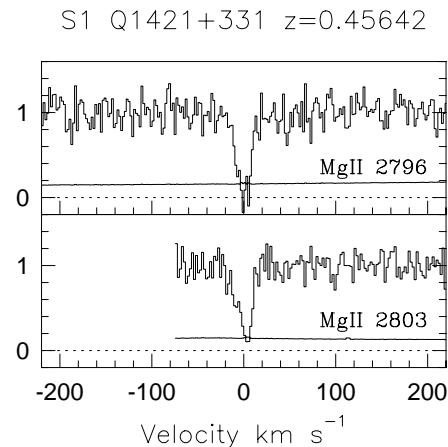


Fig. 2a.— The detected transitions of the weak MgII systems. All detections are 5σ unless annotated otherwise. Absorption features marked with “*” are not associated with the system being presented. In systems with multiple components, ticks mark the components that are detected at the 3σ level.

S2 Q1329+412 $z=0.50079$

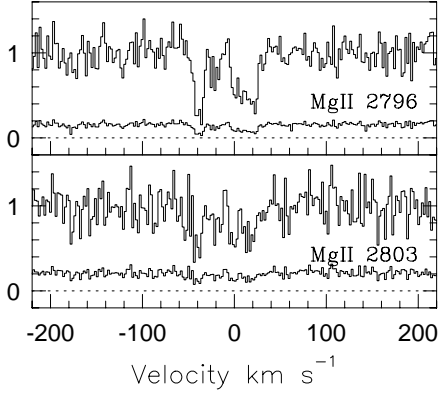


Fig. 2*b*.— Same as for figure 2*a*

S5 Q1241+174 $z=0.55844$

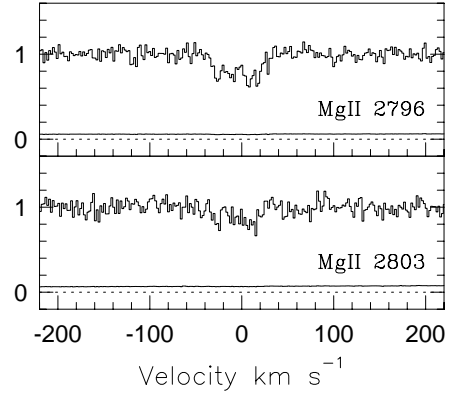


Fig. 2*e*.— Same as for figure 2*a*

S3 Q1354+193 $z=0.52150$

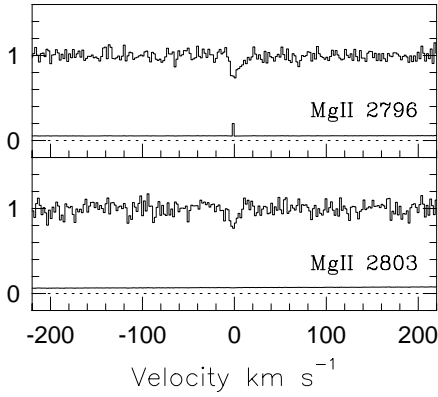


Fig. 2*c*.— Same as for figure 2*a*

S4 Q1222+228 $z=0.55020$

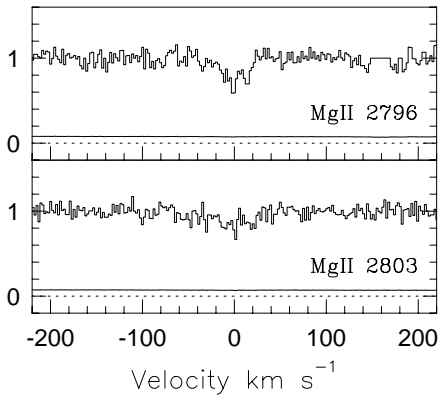


Fig. 2*d*.— Same as for figure 2*a*

S6 Q0002+051 $z=0.59149$

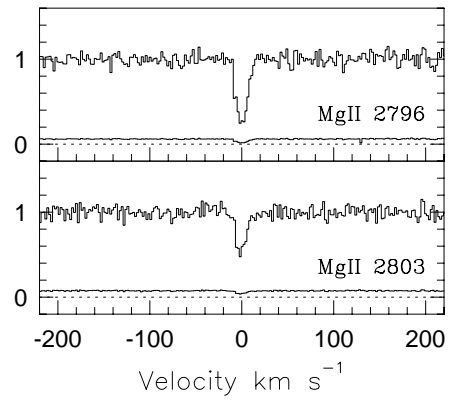


Fig. 2*f*.— Same as for figure 2*a*

S7 Q0454+039 $z=0.64283$

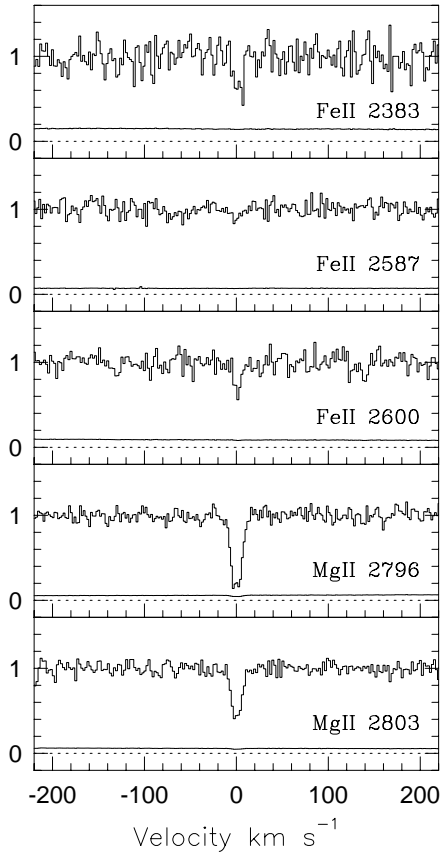


Fig. 2g.— Same as for figure 2a

S8 Q0823-223 $z=0.70547$

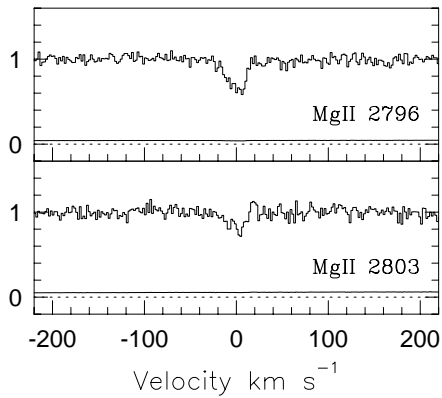


Fig. 2h.— Same as for figure 2a

S9 Q0058+019 $z=0.72518$

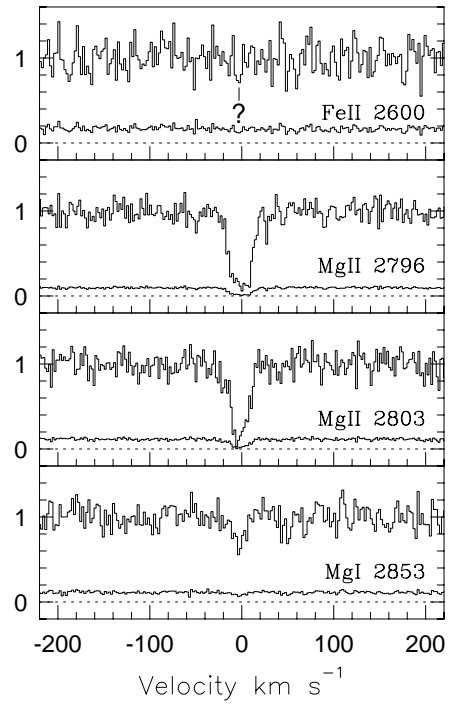


Fig. 2i.— Same as for figure 2a

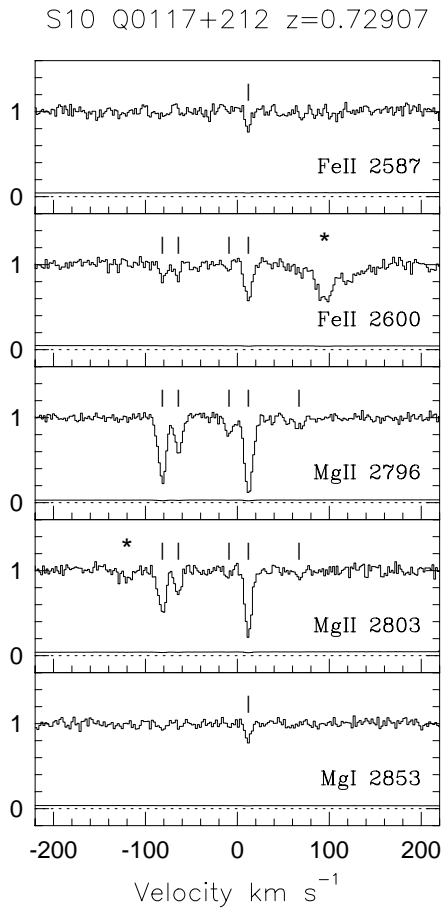


Fig. 2j.— Same as for figure 2a

S11 Q1548+092 $z=0.77065$

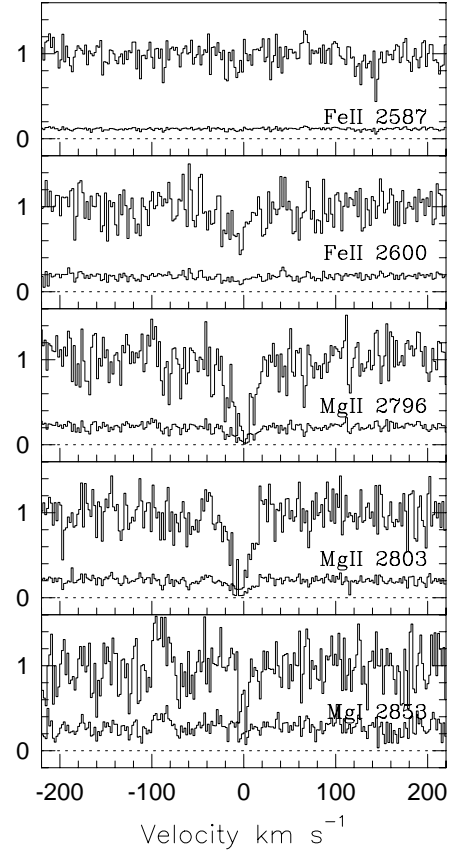


Fig. 2k.— Same as for figure 2a

S12 Q1634+706 $z=0.81816$

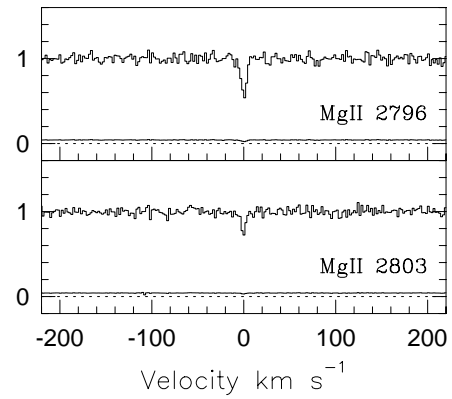


Fig. 2l.— Same as for figure 2a

S13 Q1421+331 $z=0.84325$

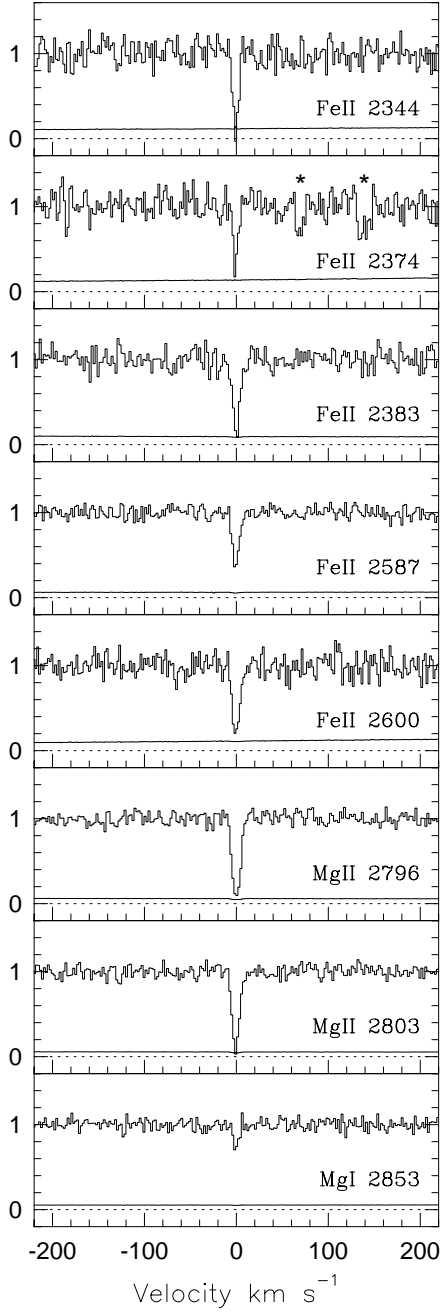


Fig. 2m.— Same as for figure 2a

S14 Q1248+401 $z=0.85455$

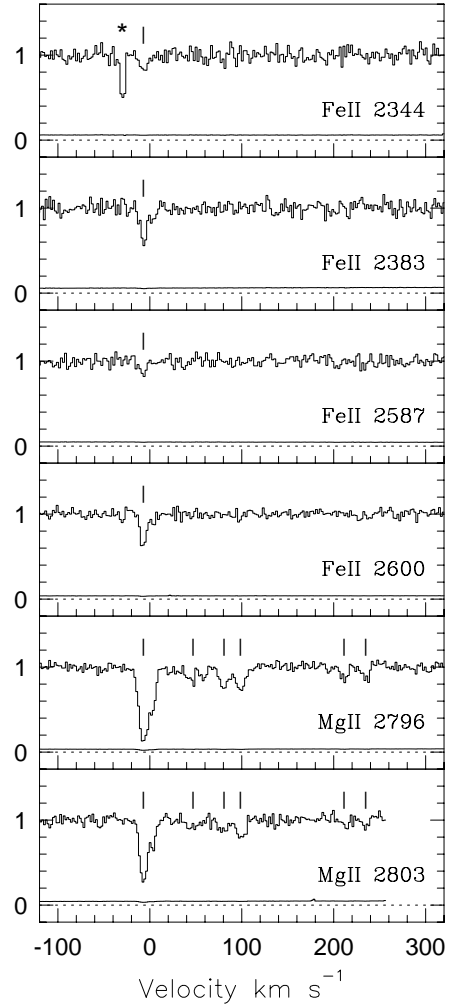


Fig. 2n.— Same as for figure 2a

S15 Q0002+051 $z=0.86653$

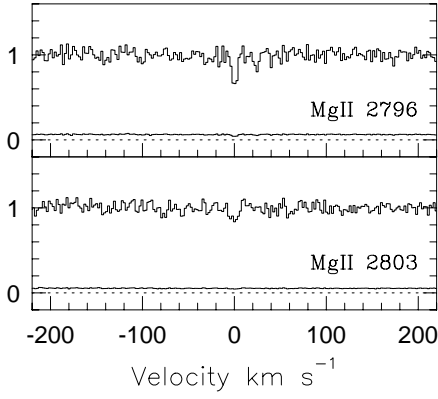


Fig. 2o.— Same as for figure 2a

S16 Q1241+174 $z=0.89549$

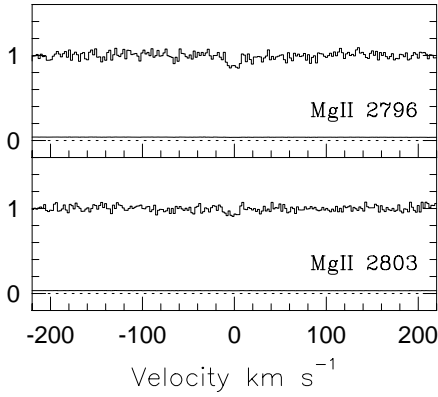


Fig. 2p.— Same as for figure 2a

S17 Q1634+706 $z=0.90555$

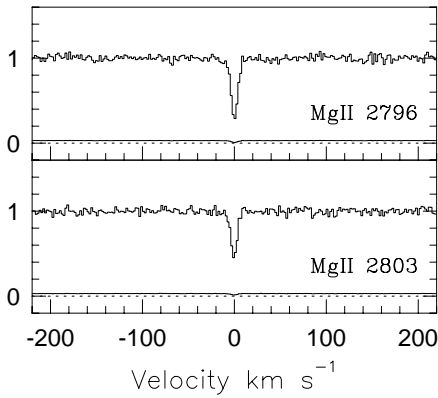


Fig. 2q.— Same as for figure 2a

S18 Q0454+039 $z=0.93150$

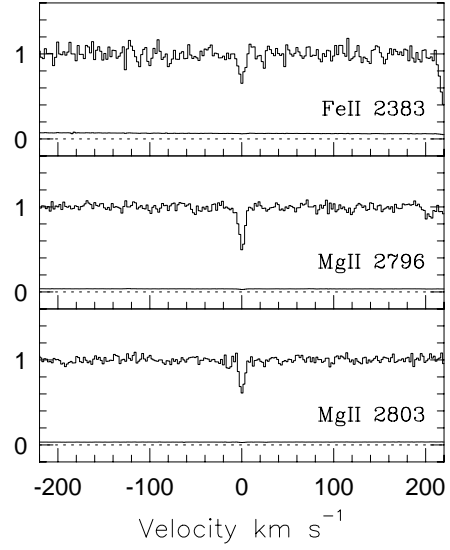


Fig. 2r.— Same as for figure 2a

S19 Q1206+459 $z=0.93428$

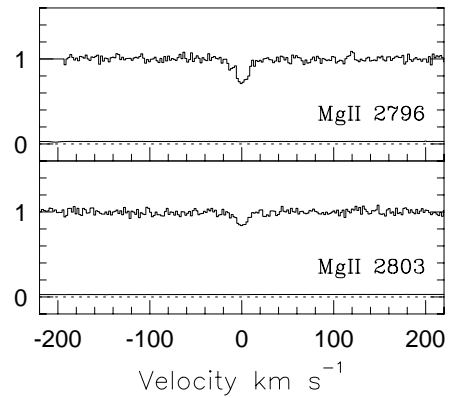


Fig. 2s.— Same as for figure 2a

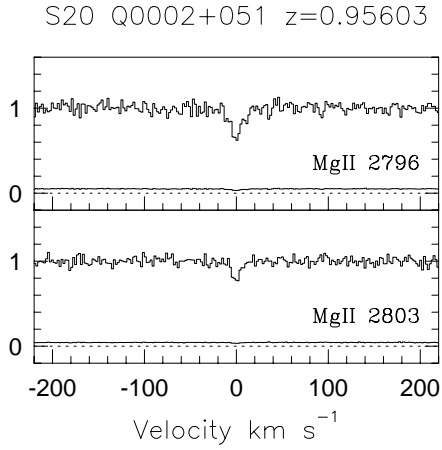


Fig. 2*t*.— Same as for figure 2*a*

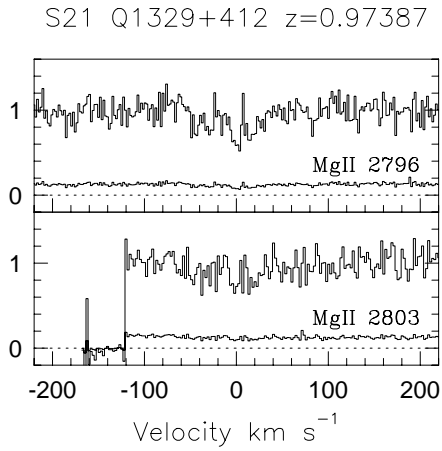


Fig. 2*u*.— Same as for figure 2*a*

S22 Q1329+412 $z=0.99836$

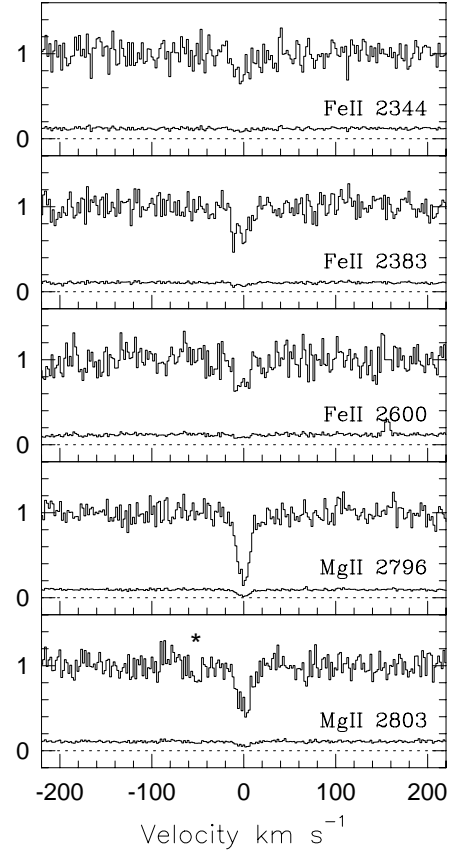


Fig. 2*v*.— Same as for figure 2*a*

S23 Q1634+706 $z=1.04144$

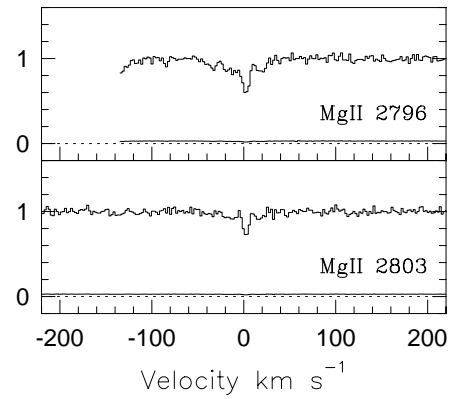


Fig. 2*w*.— Same as for figure 2*a*

S24 Q1213-003 $z=1.12770$

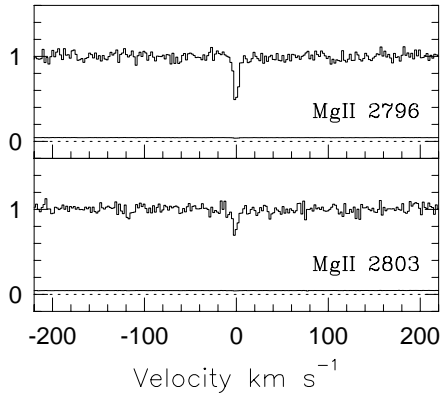


Fig. 2x.— Same as for figure 2a

S25 Q0958+551 $z=1.21132$

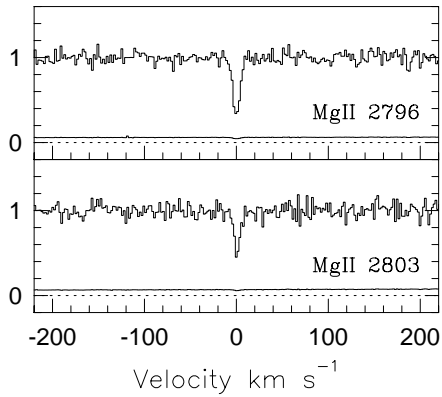


Fig. 2y.— Same as for figure 2a

S26 Q0450-132 $z=1.22948$

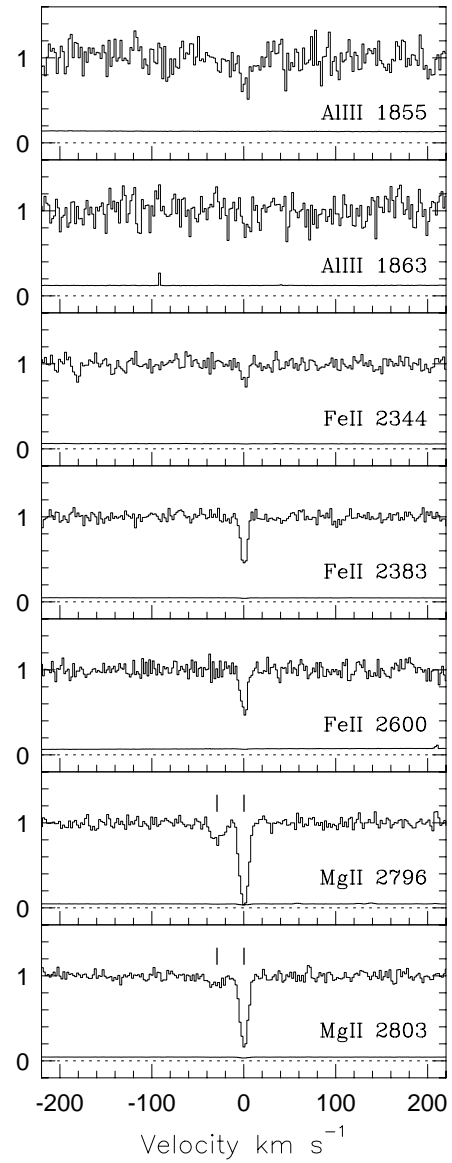


Fig. 2z.— Same as for figure 2a

S27 Q0450-132 $z=1.23244$

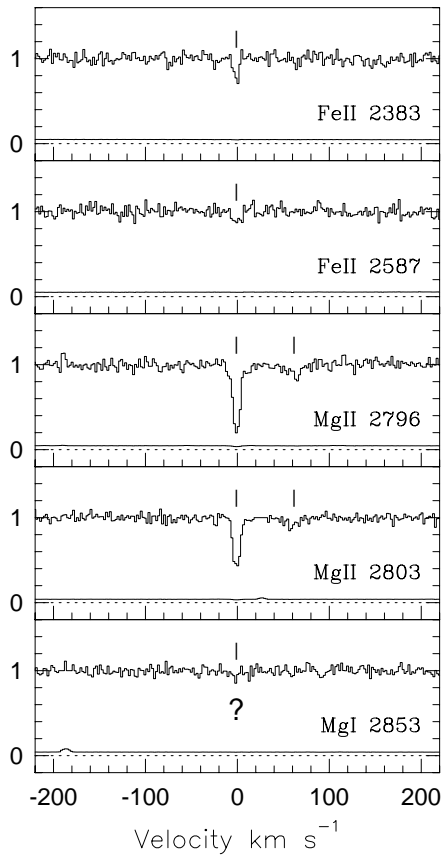


Fig. 2aa.— Same as for figure 2a

S28 Q0958+551 $z=1.27238$

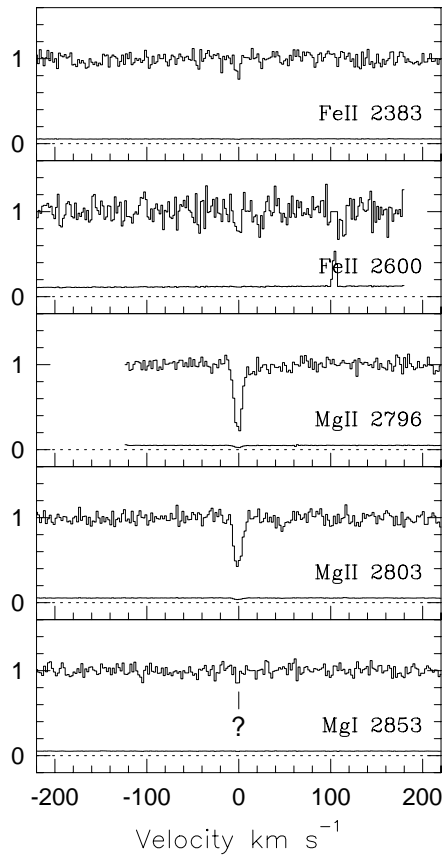


Fig. 2bb.— Same as for figure 2a

S29 Q0117+212 $z=1.32500$

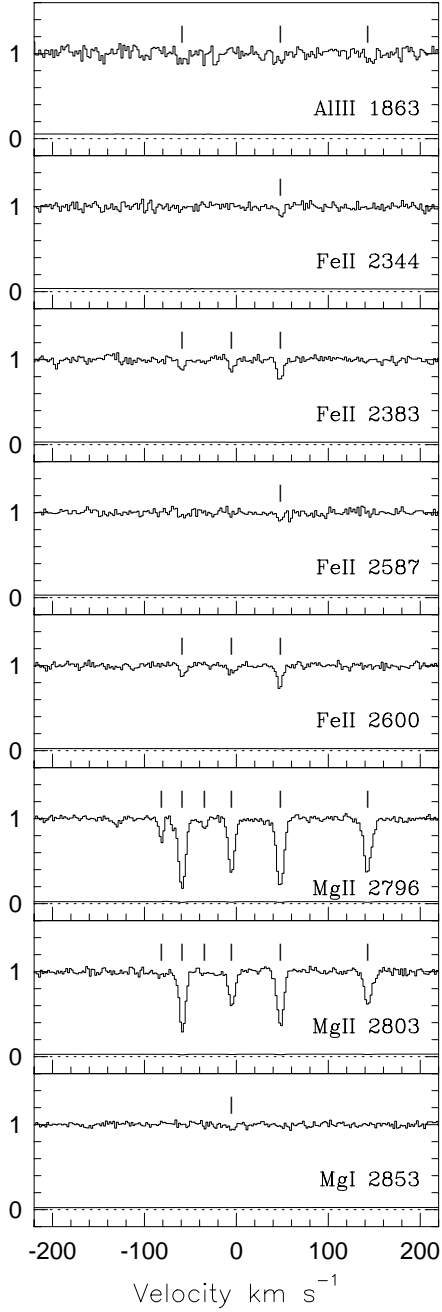


Fig. 2cc.— Same as for figure 2a

S30 Q0117+212 $z=1.34297$

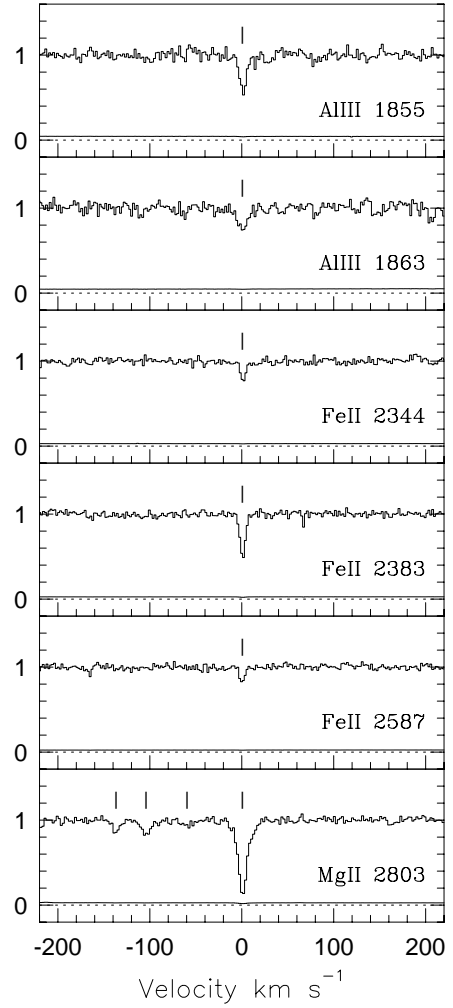


Fig. 2dd.— Same as for figure 2a

3.1.4. S4 (Q1222 + 228; $z_{\text{abs}} = 0.550202$)

There is no previous report of S4. Though FeII and MgI were captured by the CCD, only the MgII doublet was detected. However, FeII $\lambda 2600$ may be present at the 2.7σ level. A CIV detection was ambiguous in the FOS/*HST* spectrum (also see Impey et al. 1996); we conservatively quote a non-restrictive limit. There is no galaxy candidate (C. Steidel, private communication).

3.1.5. S5 (Q1241 + 174; $z_{\text{abs}} = 0.55844$)

There is no previous report of S5. Though FeII and MgI were captured by the CCD, only the MgII doublet was detected. CIV was tentatively detected in the FOS/*HST* spectrum; however, the $\lambda 1548$ line may be Ly α (Jannuzi et al. 1998). There is no galaxy candidate (C. Steidel, private communication).

3.1.6. S6 (Q0002 + 051; $z_{\text{abs}} = 0.59149$)

S6 is known to be associated with a red $\simeq 1.3L_K^*$ galaxy with impact parameter $\simeq 24h^{-1}$ kpc (Churchill, Steidel, & Vogt 1996). Though multiple FeII transitions were captured by the CCD, none were detected. If MgI is present, it was detected only at the 2σ significance level. The equivalent widths may be biased by a zero-point uncertainty, which has not been included in the error measurement. CIV was not detected in the FOS/*HST* spectrum (also see Jannuzi et al. 1998).

3.1.7. S7 (Q0454 + 036; $z_{\text{abs}} = 0.64283$)

S7 was studied by Churchill & Le Brun (1998) and has no detectable CIV in the FOS/*HST* spectrum. There is no galaxy at this redshift in this well studied field. Here, we also report a 3.3σ detection of FeII $\lambda 2587$. MgI was not detected.

3.1.8. S8 (Q0823 – 223; $z_{\text{abs}} = 0.705472$)

There is no previous report of S8. Though FeII and MgI were captured by the CCD, only the MgII doublet was detected. CIV was not detected in the FOS/*HST* spectrum.

3.1.9. S9 (Q0058 + 019; $z_{\text{abs}} = 0.72518$)

There is no previous report of S9. Relatively strong MgI was detected. There is a 3σ detection of FeII $\lambda 2600$, which we present in Table 3, but this detection is insecure. A FOS/*HST* spectrum of this QSO was not available. There is no galaxy candidate, though

there is a galaxy at $z \simeq 0.68$ (C. Steidel, private communication).

3.1.10. S10 (Q0117 + 212; $z_{\text{abs}} = 0.72907$)

S10, a multi-component system, is associated with a red and massive $\simeq 3.7L_K^*$ galaxy at an impact parameter of $\simeq 36h^{-1}$ kpc (Churchill et al. 1996). The absorption at $v \simeq -120$ km s^{-1} near the $\lambda 2803$ transition is a TiII transition from a damped Ly α absorber at $z_{\text{abs}} = 0.5764$. Also, FeII $\lambda 2600$ is nearly blended with MgI from this damped Ly α absorber. FeII has been detected in four of the five MgII components and MgI was detected in the strongest one. CIV was not detected in the FOS/*HST* spectrum (also see Jannuzi et al. 1998).

3.1.11. S11 (Q1548 + 093; $z_{\text{abs}} = 0.77065$)

SSB reported a weak, but unambiguous, MgII absorbing system at $z_{\text{abs}} = 0.7708$. This system is associated with a reddish low mass galaxy with $\simeq 0.1L_K^*$ at an impact parameter of $\simeq 23h^{-1}$ kpc (C. Steidel, private communication). Though the HIRES spectrum is noisy, both FeII and MgI were detected. A FOS/*HST* spectrum of this QSO was not available.

3.1.12. S12 (Q1634 + 706; $z_{\text{abs}} = 0.81816$)

There is no previous report of S12. The MgII is very weak, with $W_r(2796) = 0.03$ Å. There is no detection of MgI, where the signal-to-noise ratio is quite high, nor of FeII. CIV was not detected in the FOS/*HST* spectrum (also see Bahcall et al. 1996).

3.1.13. S13 (Q1421 + 331; $z_{\text{abs}} = 0.84325$)

There is no previous report of S13. However, Uomoto (1984) reported two unidentified weak lines in his low resolution spectrum; these two lines correspond to FeII $\lambda 2600$ and $\lambda 2374$ at this redshift. This system is very rich in FeII transitions. Also, MgI was detected. A FOS/*HST* spectrum of this QSO was not available.

3.1.14. S14 (Q1248 + 401; $z_{\text{abs}} = 0.85455$)

There is no previous report of S14, which exhibits multiple components. FeII was detected only in the strongest MgII component. CIV was reported by Jannuzi et al. (1998) in the FOS/*HST* spectrum and is confirmed in our search. There is no galaxy candidate (C. Steidel, private communication).

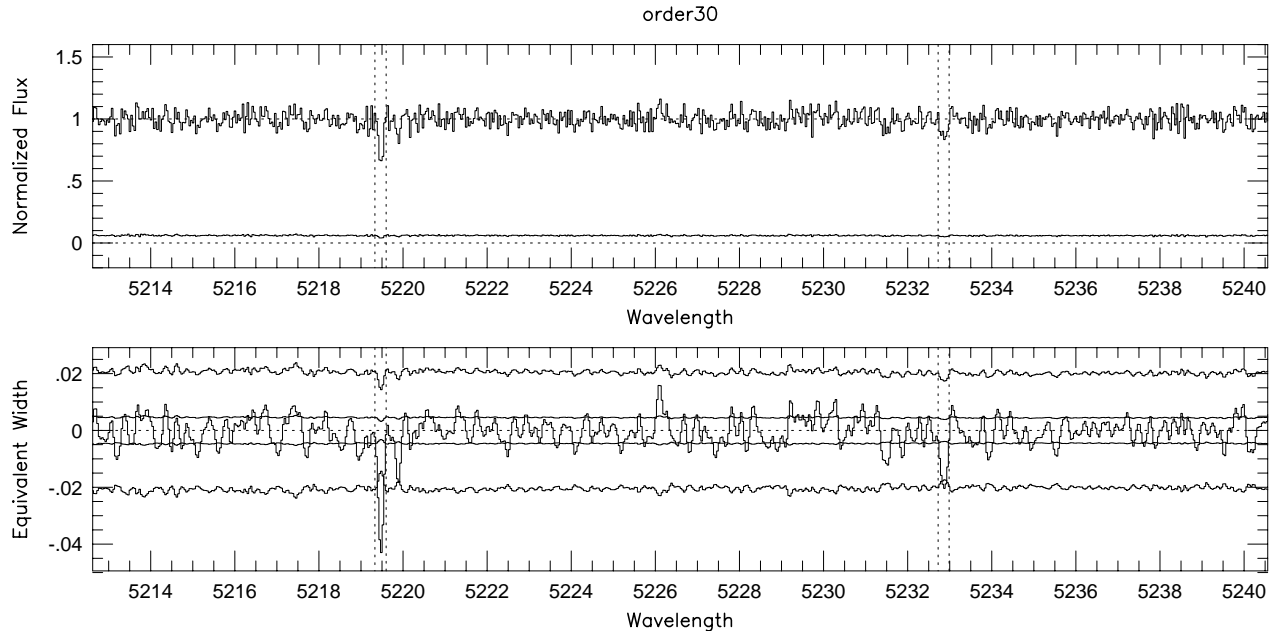


Fig. 3.— The S15 MgII doublet detection (5σ) illustrated from our detection software. S15 is the weakest system in the sample and the (unresolved) profile shapes of the $\lambda 2796$ and $\lambda 2803$ transitions are quite different, with the $\lambda 2803$ profile being broader. This system provides an example of the detection sensitivity of our doublet searching algorithm. The limiting observed equivalent width on this order is roughly 0.02 \AA , which corresponds to 0.011 \AA in the rest frame of the $\lambda 2796$ transition at these wavelengths. The top panel shows the spectrum and the uncertainty spectrum. The lower panel shows the equivalent width spectrum (average of zero). Pixels with positive equivalent widths are emission features and those with negative equivalent widths are absorption features. The uncertainty in the equivalent width spectrum is shown at both 1σ (inner) and 5σ (outer) levels. A feature is objectively identified when a pixel has an equivalent width that is larger than the 5σ uncertainty. The vertical dashed lines are to illustrate the locations of the identified features.

3.1.15. S15 (Q0002 + 051; $z_{\text{abs}} = 0.86653$)

There is no previous report of S15. This is the weakest system in our survey, with $W_r(2796) = 0.018 \text{ \AA}$. In Figure 3, we show the detection of this system. FeII and MgI were captured by the CCD, but neither was detected. The equivalent widths may be biased by a zero-point uncertainty, which has not been included in the error measurement. CIV was not detected in the FOS/*HST* spectrum (also see Jannuzi et al. 1998). The Q0002 + 051 field has been studied in detail and there is no galaxy (to roughly $0.2L_K^*$) observed at this redshift within $20''$ of the QSO (C. Steidel, private communication).

3.1.16. S16 (Q1241 + 174; $z_{\text{abs}} = 0.89549$)

There is no previous report of S16. Neither FeII nor MgI were detected. CIV was not detected in the FOS/*HST* spectrum (also see Jannuzi et al. 1998). There is no galaxy candidate (C. Steidel, private communication).

3.1.17. S17 (Q1634 + 706; $z_{\text{abs}} = 0.90555$)

There is no previous report of detected MgII in S17, though CIV was reported by Bergeron (1994) and Bahcall et al. (1996). MgI was not detected, where the signal-to-noise ratio is high, nor was FeII.

3.1.18. S18 (Q0454 + 036; $z_{\text{abs}} = 0.93150$)

S18 was studied by Churchill & Le Brun (1998), who found no CIV in the FOS/*HST* spectrum and

no galaxy at this redshift. FeII λ 2383 was detected, and FeII λ 2600 would likely have been detected, but the region of the spectrum was compromised by the pen mark on the HIRES CCD. There is a tentative detection (2.7σ) of FeII λ 2587. MgI was not detected.

3.1.19. S19 (Q1206 + 456; $z_{\text{abs}} = 0.93428$)

S19 was studied by Churchill & Charlton (1998). No FeII transitions were detected, nor was MgI. S19 may be a member of a small group of galaxies. Kirhakos et al. (1992) identified ten galaxies within a $100''$ of the QSO, three of which are within $10''$. Thimm (1995) found strong [OII] λ 3727 emission at $z = 0.93$ from one of these galaxies. In the FOS/*HST* spectrum, CIV and OVI are clearly present (see Jannuzi et al. 1998; Churchill & Charlton 1998).

3.1.20. S20 (Q0002 + 051; $z_{\text{abs}} = 0.95603$)

There is no previous report of S20. Neither FeII nor MgI was detected. The equivalent widths may be biased by a zero-point uncertainty, which has not been included in the error measurement. CIV was detected in the FOS/*HST* spectrum (also see Jannuzi et al. 1998). The Q0002 + 051 field has been studied in detail and there is no galaxy (to roughly $0.2L_K^*$) observed at this redshift within $20''$ of the QSO (C. Steidel, private communication).

3.1.21. S21 (Q1329 + 412; $z_{\text{abs}} = 0.97387$)

There is no previous report of S21. The λ 2803 transition is near the CCD edge. FeII was not detected. MgI may have been detected, but only at the 2.5σ level. A non-restrictive limit was placed in CIV, which falls in the Ly α forest in the FOS/*HST* spectrum. There is no galaxy candidate (C. Steidel, private communication).

3.1.22. S22 (Q1329 + 412; $z_{\text{abs}} = 0.99836$)

There is no previous report of S22. The system has strong FeII absorption. MgI was not captured by the CCD. CIV was not detected in the FOS/*HST* spectrum. There is no galaxy candidate (C. Steidel, private communication).

3.1.23. S23 (Q1634 + 706; $z_{\text{abs}} = 1.04144$)

There is no previous report of detected MgII in S23, though CIV was reported by Bergeron et al. (1994)

and Bahcall et al. (1996). Even at very high signal-to-noise ratio, neither FeII nor MgI was detected.

3.1.24. S24 (Q1213 – 003; $z_{\text{abs}} = 1.12770$)

There is no previous report of S24. This system had a “false alarm” probability of $P_{\text{fa}} = 0.009$, the largest in the sample. FeII λ 2383 may have been detected at the 3σ level, but there are two nearby 3σ features. We conservatively quote a limit. A ground-based spectrum covering CIV was not found in the literature.

3.1.25. S25 (Q0958 + 551; $z_{\text{abs}} = 1.21132$)

There is no previous report of S25. Neither FeII nor MgI was detected. A ground-based spectrum covering CIV was not found in the literature.

3.1.26. S26 (Q0450 – 132; $z_{\text{abs}} = 1.22948$)

S26, a multi-component system, was reported by SS92. The system is strong in FeII absorption in the strongest MgII component. The AlIII λ 1855, 1863 doublet was detected in the strongest component (also see Petitjean, Rauch, & Carswell 1994). This is the lowest redshift system in which AlIII was covered. MgI was not detected. A ground-based spectrum covering CIV was not found in the literature.

3.1.27. S27 (Q0450 – 132; $z_{\text{abs}} = 1.23244$)

There is no previous report of S27. The MgII profiles is in two components. FeII and MgI were detected in the narrow component. However, the MgI detection is ambiguous. A ground-based spectrum covering CIV was not found in the literature.

3.1.28. S28 (Q0958 + 551; $z_{\text{abs}} = 1.27238$)

There is no previous report of S28. FeII was detected; however, the λ 2600 equivalent width is unphysically large with respect to the more robust λ 2383 equivalent width. MgI was detected, but is deemed uncertain. Sargent, Boksenberg, & Steidel (1988) reported CIV at this redshift.

3.1.29. S29 (Q0117 + 212; $z_{\text{abs}} = 1.32500$)

S29 was reported by SS92. The system is comprised of five distinct components. FeII was detected in three of the five components. AlIII λ 1863 was also detected in three components; AlIII λ 1855 was not

captured by the CCD. MgI was detected in the weakest MgII component, and in this component there is no AlIII. CIV absorption was reported by SS92, though the doublet was not resolved. There are candidate galaxies for this system (C. Steidel, private communication).

3.1.30. S30 (Q0117 + 212; $z_{\text{abs}} = 1.34297$)

S30 was also reported by SS92. Only the $\lambda 2803$ transition of the MgII doublet was captured. As such, this system would not have been detected in our unbiased doublet search. It is not a member of our adopted sample nor was it included in any of the system statistics. The MgII profile is comprised of four components. MgI was not detected. FeII was detected in the dominant, but narrow, MgII component. Also, AlIII was found in this component. CIV was reported by SS92, though the doublet was not resolved. There are candidate galaxies for this system (C. Steidel, private communication).

3.2. Survey Completeness

To evaluate the completeness of the survey as a function of redshift we have adopted the formalism used by SS92 and LTW, namely the “redshift path density”, $g(W, z)$. This function gives the number of sight lines along which a MgII $\lambda 2796$ transition at redshift z and with rest-frame equivalent width greater than or equal to W could have been discovered. Because of the high resolution of the spectra, we have slightly modified the computation of the redshift path density to include sensitivity to the MgII doublet ratio. Thus, we have $g(W, z, \text{DR})$, the number of sight lines along which a MgII *doublet* at redshift z with $\lambda 2796$ rest-frame equivalent width greater than or equal to W , and with doublet ratio less than DR could have been detected.

The cumulative redshift path length covered by the survey over a given redshift interval is then

$$Z(W_r, \text{DR}) = \int_{z_1}^{z_2} g(W_r, z, \text{DR}) dz, \quad (2)$$

where we have chosen not to integrate from $0 \leq z \leq \infty$ because our $g(W_r, z, \text{DR})$ drops dramatically for $z_1 < 0.4$ and for $z_2 > 1.4$. In Figure 4, we have plotted the cumulative redshift path of the survey as a function of W_r^{min} for $\text{DR}^{\text{max}} = 1$ (dotted curve) and for $\text{DR}^{\text{max}} = 2$ (solid curve). It is apparent that the redshift path, and thus the survey completeness, is

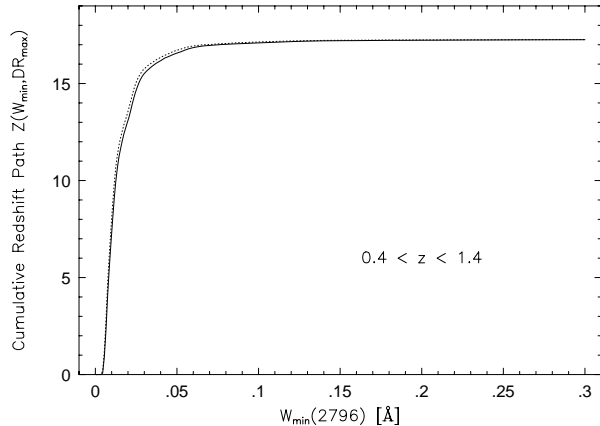


Fig. 4.— The redshift path of the survey over the redshift interval $0.4 \leq z \leq 1.4$ versus the rest-frame MgII $\lambda 2796$ equivalent width threshold for a 5σ detection level. The dotted curve is for unit doublet ratio and the solid curve is for $\text{DR} = 2$.

not sensitive to the doublet ratio. We are 91% complete at $W_r(2796) = 0.03 \text{ \AA}$ (5σ), and 80% complete at $W_r(2796) = 0.02 \text{ \AA}$. For comparison, SS92 were 83% complete at $W_r(2796) = 0.3 \text{ \AA}$.

4. The Statistical Properties of Weak MgII Absorbers

4.1. Redshift Number Density

Since we are unbiased only for $W_r(2796) < 0.3 \text{ \AA}$, we calculated the number of absorbers per unit redshift, dN/dz , for this limited range using the formalism of LTW. From Eq. 2, we computed the redshift path length, $Z(W_i, \text{DR}_i)$, over which the i th system could have been detected in our survey. The values are presented in Table 2. The number per unit redshift path is simply the sum of the reciprocal of the cumulative redshift path lengths,

$$\frac{dN}{dz} = \sum_i^{N_{\text{sys}}} [Z(W_i, \text{DR}_i)]^{-1}. \quad (3)$$

The variance in dN/dz is given by

$$\sigma_{dN/dz}^2 = \sum_i^{N_{\text{sys}}} [Z(W_i, \text{DR}_i)]^{-2}. \quad (4)$$

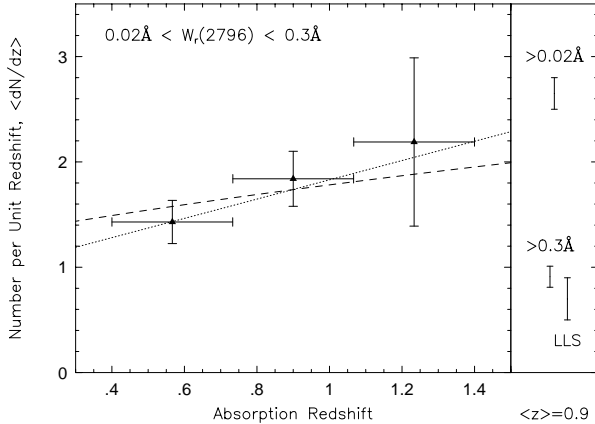


Fig. 5.— (left panel) The number of MgII systems per unit redshift, dN/dz , with $0.02 \leq W_r(2796) < 0.3 \text{ \AA}$ for three redshift bins over the interval $0.4 \leq z \leq 1.4$. The vertical error bars are the Poisson uncertainties in the dN/dz and the horizontal give the redshift bins. The dotted curve is the no-evolution expectations for $q_0 = 0$ and the dashed curve is for $q_0 = 0.5$, where the curves have been normalized at $z = 0.9$ (see text). — (right panel) A comparison of the MgII dN/dz for different $\lambda 2796$ equivalent width cut offs with the LLS dN/dz . The $W_r(2796) \geq 0.3 \text{ \AA}$ number is taken from SS92, and the Lyman limit data are taken from Stengler-Larrea et al. (1995).

Over the redshift range $0.4 \leq z \leq 1.4$, we obtained

$$\frac{dN}{dz} = 1.74 \pm 0.11 \quad \text{for } 0.02 \leq W_r(2796) < 0.3 \text{ \AA}, \quad (5)$$

where $\langle z \rangle = 0.9$. In the left hand panel of Figure 5, we have plotted dN/dz versus redshift for $0.02 \leq W_r(2796) < 0.3 \text{ \AA}$, for three redshift bins, [0.40, 0.74], [0.74, 1.07], and [1.07, 1.40]. The curves represent the no-evolution expectations for $q_0 = 0.5$ (dashed curve) and for $q_0 = 0$ (dotted curve) normalized to $dN/dz = 1.74$ at $z = 0.9$. We have assumed the standard parameterization, $dN/dz = N_0(1+z)^\gamma$, where $\gamma = 1$ for $q_0 = 0$ and $\gamma = 0.5$ for $q_0 = 0.5$. A formal fit yielded $\gamma = 1.3 \pm 0.9$ and $N_0 = 0.8 \pm 0.4$. The data are not inconsistent with the no-evolution expectations for either q_0 . In the right hand panel of Figure 5, we have plotted the mean dN/dz and its uncertainty at $\langle z \rangle = 0.9$ for: (1) the $W_r^{\min}(2796) = 0.3 \text{ \AA}$ MG1 sample of SS92, which has $dN/dz = 0.91 \pm 0.10$; (2) the combined $W_r^{\min}(2796) = 0.02 \text{ \AA}$ sample, which

has $dN/dz = 2.65 \pm 0.15$; and (3), the *HST* Key Project results for a sample of Lyman limit systems (LLS), which has $dN/dz = 0.7 \pm 0.2$ over the interval $0.4 \leq z \leq 1.4$ (Stengler-Larrea et al. 1995).

Taken at face value, these numbers imply that weak MgII absorbers comprise $\sim 65\%$ of the total MgII absorber population and that the vast majority of them must arise in sub-LLS environments. We return to this point in §5.1. The dN/dz of weak MgII absorbers is roughly 5–7% of that of the Ly α forest with $W_r(\text{Ly}\alpha) \geq 0.1 \text{ \AA}$ (Jannuzi et al. 1998). We tentatively suggest that $\sim 5\%$ of $z \leq 1$ “Ly α forest clouds” with $0.1 \leq W_r(\text{Ly}\alpha) \leq 1.6 \text{ \AA}$ will exhibit MgII absorption to a 5σ $W_r(2796)$ detection limit of 0.02 \AA . The two MgII systems found by Churchill & Le Brun (1998) in a search through 28 forest clouds in the spectrum of PKS 0454 + 039 are consistent with these expectations.

4.2. Equivalent Width Distribution

The distribution function, $n(W)$, is defined as the number of MgII absorption systems with equivalent width W per unit equivalent width per unit redshift path. It has been customary to parameterize the distribution by either an exponential,

$$n(W)dW = \left(\frac{N^*}{W^*}\right) \exp\left(-\frac{W}{W^*}\right) dW, \quad (6)$$

or a power law,

$$n(W)dW = CW^{-\delta}dW, \quad (7)$$

where N^* and W^* (for the exponential) and C and δ (for the power law) are parameters obtained by fitting the data. TBSYK fit the distribution with a power law of $\delta \sim 2$ for a sample with $W_r^{\min}(2796) = 0.25 \text{ \AA}$ and mean redshift $\langle z \rangle \simeq 0.5$. For $W_r^{\min}(2796) = 0.3 \text{ \AA}$ systems at $\langle z \rangle \simeq 1.6$, LTW fit the distribution to both an exponential and a power-law distribution (the latter in agreement with TBSYK). LTW concluded that both adequately represented the data, with the exponential distribution slightly favored. SS92 found that $n(W)$ could be parameterized tolerably well by either an exponential, with $N^* \sim 1.5$ and $W^* \sim 0.66$, or by a power law, with $C \sim 0.4$ and $\delta \simeq 1.65$. SS92 noted that the exponential underpredicted the number of $W_r(2796) \leq 0.5 \text{ \AA}$ systems whereas the power law underpredicted the number with “intermediate” equivalent widths, those with $0.7 \leq W_r(2796) \leq 1.3 \text{ \AA}$.

In Figure 6a and b, we present $n(W_r)$ for $W_r(2796) \geq 0.0165 \text{ \AA}$. We are 70% complete to this equivalent

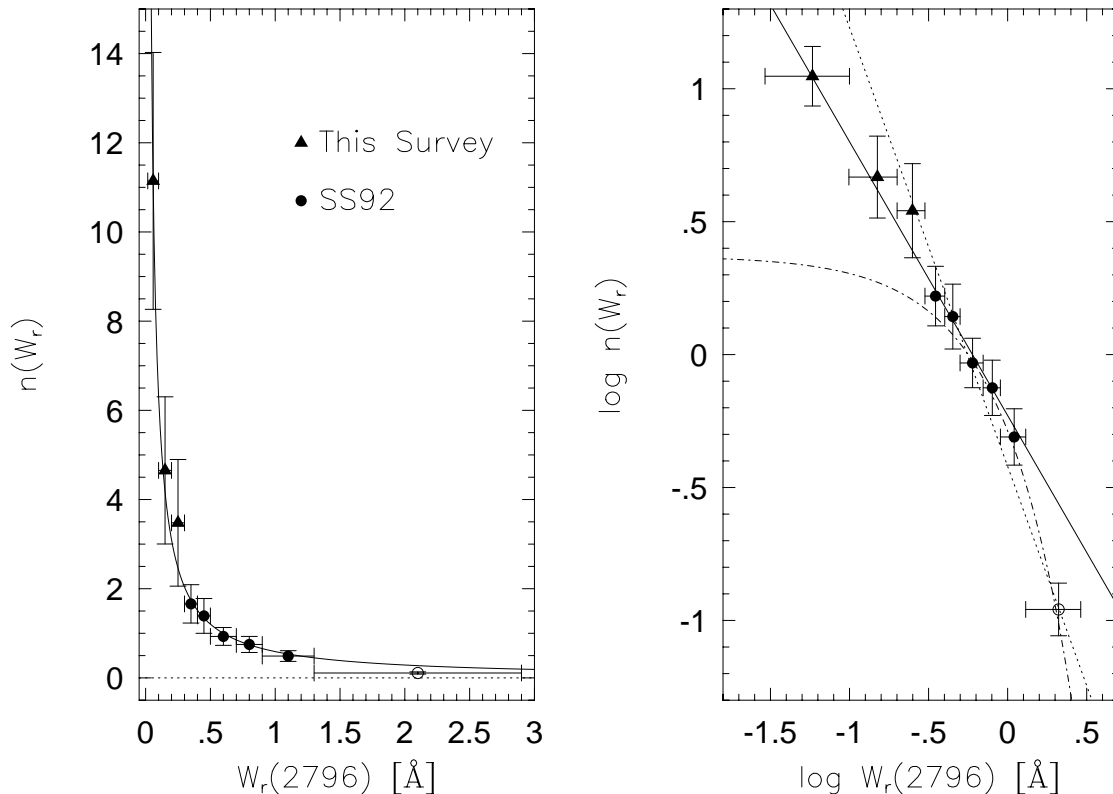


Fig. 6.— The equivalent width distribution versus the rest-frame equivalent width of the MgII $\lambda 2796$ transition. The left hand panel illustrates the rapid increase in the number of small $W_r(2796)$ systems. Solid triangles are from this study and solid circles are taken from SS92. The right hand panel shows a comparison of our power-law fit (solid line) to the combined data set from this study and SS92. Also shown are the fits presented by SS92 for a power law (dot-dash) and an exponential (dash-dot). The largest equivalent widths [$W_r(2796) \geq 1.3$ Å; shown with an open dot] from the SS92 data are predominantly from redshifts higher than $z = 1.4$, our upper cut off. Due to the evolution of the strongest systems, this binned data point would be lower if the SS92 data were limited to our redshift coverage (see the text).

width. Solid triangles are the results from our survey. The data have been binned accounting for the redshift path length over which the equivalent widths could have been detected. The three equivalent width bins are $[0.0165, 0.1]$, $[0.1, 0.2]$, and $[0.2, 0.3]$ Å. Shown as solid circles are the binned equivalent width data from SS92 (see their Figure 6), which span the range $0.3 \leq W_r(2796) \leq 2.8$ Å. Figure 6a illustrates the dramatic increase in $n(W_r)$ with decreasing equivalent width. *There is no turnover or break in the equivalent width distribution for $0.02 \leq W_r(2796) < 0.3$ Å at $\langle z \rangle = 0.9$.*

The lack of a turnover is further illustrated in Figure 6b, which shows $\log n(W_r)$ versus $\log W_r(2796)$. The solid curve is a power law with $\delta = 1.04$, which was obtained by minimizing the absolute deviation between the curve (Eq. 7) and the binned data. The

absolute deviation for the presented fit is 0.07 (in log-log). This fit is also presented in Figure 6a. It would be proper to fit the combined data of this survey and SS92 using the maximum likelihood technique employed by LTW, TBSYK, and SS92. This would require that we invoke the $g(W, z)$ function of SS92 and reanalyze the SS92 data over the redshift interval $0.4 \leq z \leq 1.4$. However, with this work, it is our intent to clearly demonstrate the absence of a turnover in the equivalent width distribution at small equivalent widths and to discern between the exponential and power-law parameterizations of the distribution. A reanalysis of the SS92 data was not required to demonstrate these points.

Neither Eq. 6 nor 7 accounts for redshift evolution in the distribution. However, such evolution has been observed. TBSYK found evidence for

more large equivalent width absorbers at high redshift than at low redshift. PB90 noted that the ratio of “weak” to “strong” absorbers, demarcated by $W_r(2796) = 0.6 \text{ \AA}$, increased with decreasing redshift. SS92 measured how the number density evolution of MgII systems changed as a function of $W_r^{\min}(2796)$. As $W_r^{\min}(2796)$ is increased, evolution becomes pronounced; large equivalent width systems evolve away with time. When $W_r^{\min}(2796) = 0.3 \text{ \AA}$ is applied, the population of MgII absorbers is consistent with no-evolution expectations. It appears that the evolution of the strongest systems, those with $W_r(2796) \geq 0.6 \text{ \AA}$, may have strongly biased the SS92 fits to the equivalent width distribution (a point they address in their paper). Slightly more than 60% of the equivalent widths¹¹ contributing to the largest bin ($[1.3, 2.8] \text{ \AA}$) taken from SS92 arise at $z \geq 1.4$. We have plotted this bin as an open circle in Figures 6a and 6b. If we had corrected this bin for our limited redshift coverage, it would be roughly 40% of its plotted value ($\log n \sim -1.46$, which is off the bottom of Figure 6b). There is no compelling evidence of such strong evolution in the equivalent width distribution for $0.3 \leq W_r(2796) \leq 1.3 \text{ \AA}$. Thus, we have omitted the $[1.3, 2.8] \text{ \AA}$ bin from our fit, and include only the bins for which evolution is thought to be negligible. To emphasize our point, we note that SS92 obtained a significantly steeper power law ($\delta = 1.65$) than the one we quote here ($\delta = 1.04$). This is likely due to the fact that the distribution of SS92 was fit over the full redshift range $0.2 \leq z \leq 2.2$, resulting in a bias from the relative paucity of large equivalent width systems at $z \leq 1.4$. This is illustrated in Figure 6b, in which we have plotted both the power-law fit (dot-dot) and the exponential fit (dash-dot) from SS92. Note that the $W_r(2796) \leq 1.3 \text{ \AA}$ data of SS92 also appear to be best described by the $\delta = 1.04$ power law distribution.

In summary, there is no turnover in the equivalent width distribution for $W_r(2796) < 0.3 \text{ \AA}$, but there is a strong break above $W_r(2796) \simeq 1.3 \text{ \AA}$ for $z \leq 1.4$. The upper limit on the slope for $W_r(2796) \geq 1.3 \text{ \AA}$ is $\delta = 2.3$.

¹¹The estimate of 60% is based upon the observed numbers. Accounting for the relative number of sight lines observed by SS92 above and below $z = 1.4$ would raise this estimate and accentuate our point.

4.3. Clustering and the Issue of a Biased Sample

The spectra used for this study are biased toward strong MgII absorbers. If the weak MgII systems tend to cluster around the stronger systems, then it is difficult to argue that the sample of weak systems is unbiased. On the other hand, if they do not cluster about the strong systems, we can conclude that the QSO sight lines are not biased toward an overabundance of weak systems.

We have computed the two-point velocity correlation function, which is presented in Figure 7, where the thick histogram distribution is the cross-correlation function of weak systems with respect to the strong systems. There are no weak systems with velocity separations less than 1000 km s^{-1} from the strong ones, and there is no apparent signal in the velocity separations. To test if the weak systems are distributed like a random population with respect to the strong systems, we have computed the relative probability, $P(\Delta v)$, of detecting a Δv separation from each strong absorption system. Following SS92,

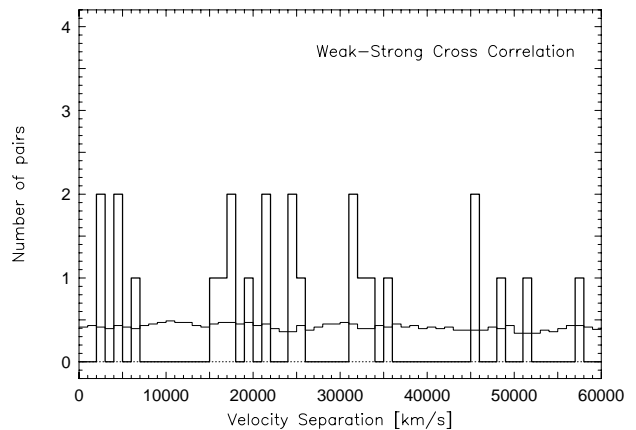


Fig. 7.— The two-point velocity cross-correlation function of weak and strong systems. Each bin gives the number of weak systems with velocity separations Δv [km s^{-1}] from strong systems along the same QSO sight line. The expected number in each bin for a random distribution is given by the thin histogram. There is no evidence that the weak systems cluster in velocity about the strong systems. This implies that the QSO sight lines, though biased for the strong systems, are in fact unbiased for the presence of weak systems.

we have limited our co-moving velocity difference to $\Delta v = 60,000 \text{ km s}^{-1}$, and have normalized the probability integral to the observed number of weak systems. Formally, the observed Δv distribution is not inconsistent with a random distribution; a χ^2 test on the binned data (1000 km s^{-1} bins) yielded a probability of 0.18 that the two distribution were drawn from the same parent population.

We examined the redshift clustering of the weak systems with respect to one another and found that it is not inconsistent with a random distribution. The χ^2 probability was 0.25. These results suggest that the weak systems are statistically consistent with a random cosmological distribution. We conclude that the QSO sight lines surveyed are unbiased for the presence of weak MgII absorbers.

4.4. Absorption Properties

A more detailed examination of the cloud to cloud chemical and ionization conditions will be presented in a companion paper (Churchill et al. 1998, Paper II). In the HIRES spectra, only MgI $\lambda 2853$, FeII $\lambda 2344$, 2374 , 2383 , 2587 , and 2600 , and the AlIII $\lambda \lambda 1855, 1863$ doublet were detected. In the FOS/*HST* spectra we have limited our search to CIV and supplemented this with measurements from ground-based observations taken from the literature. The statistics are as follows: 13 of 29 have detected FeII (either $\lambda 2383$ or $\lambda 2600$), seven of 29 have detected MgI $\lambda 2853$ and each of these also has FeII, three of four have detected AlIII, and nine of 22 have CIV. The 3σ average equivalent width threshold for FeII is 0.01 \AA for FeII $\lambda 2600$ and 0.008 \AA for FeII $\lambda 2383$. The average threshold for MgI absorption is 0.006 \AA , for AlIII is 0.01 \AA , and for CIV is 0.16 \AA .

Plotted in Figure 8 are the rest-frame MgII $\lambda 2796$ equivalent widths as a function of redshift. There appears to be no trend in the distribution of weak absorbers with redshift. We have run Spearman-Kendall (SK) non-parametric rank correlation tests to explore if any correlations are present among the detected absorption properties (limits were not included). We tested redshifts, velocity widths, equivalent widths, and doublet ratios against one another and found no correlations. The most suggestive ranking was an anti-correlation between $W_r(2796)$ and the MgII doublet ratio at the 1.4σ level. As seen in Figure 8, most, if not all, of the *individual clouds* in these weak absorbers have $W_r(2796) \leq 0.15 \text{ \AA}$. The three $W_r(2796) \geq 0.2 \text{ \AA}$ systems, S2, S9, and S11, are likely

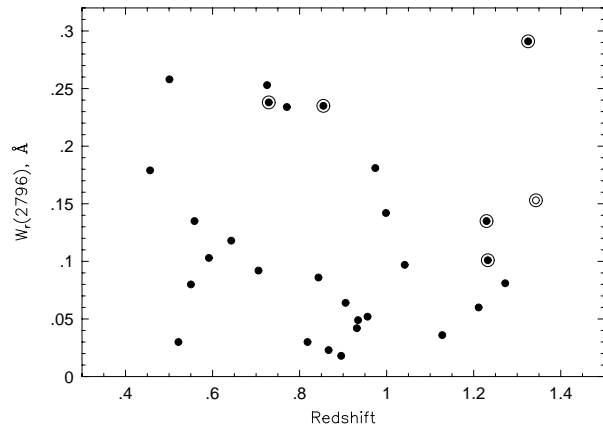


Fig. 8.— The full system rest-frame equivalent width of the MgII $\lambda 2796$ transition versus the absorption redshift. There is no evidence of any trend in $W_r(2796)$ with redshift. There is an indication that most all individual MgII absorbing clouds likely have $W_r(2796) \leq 0.15 \text{ \AA}$. Those systems that are comprised of multiple absorption features are marked with a concentric circle; the individual “cloud” $W_r(2796)$ are $\sim 0.15 \text{ \AA}$ or less. The three remaining systems with $W_r(2796) \sim 0.25 \text{ \AA}$ have relatively poor signal-to-noise ratios; they are likely to be unresolved multiple clouds. See text for discussion.

comprised of two or more blended “clouds”. In the case of S2, the profile clearly has multiple clouds.

Several of the systems have multiple components. These systems are S10, S14, S26, S27, S29, and S30. The detection of these multiple features is *not* correlated with the signal-to-noise ratio in the spectra, since they could be detected to $W_r(2796) = 0.02 \text{ \AA}$ in 80% of the systems. Plotted in Figure 9 are the velocity widths, ω_v , of the full MgII $\lambda 2796$ profiles as a function redshift. The dotted line at $\omega_v = 2.46 \text{ km s}^{-1}$, which is the Gaussian width of the instrumental profile, shows the threshold for fully unresolved features. Systems that have been resolved into multiple individual “clouds” are marked with a concentric circle. Note that the many single “cloud” systems are unresolved or only marginally resolved. The same holds true for the individual clouds in the multiple cloud systems. The average velocity width, ω_v , of the individual “clouds” for the full sample is $\sim 4 \text{ km s}^{-1}$, which implies an average temperature of $\sim 25,000 \text{ K}$ for thermal broadening. Of the

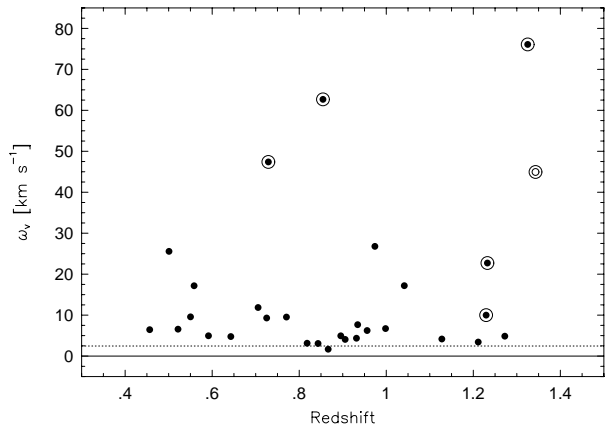


Fig. 9.— The velocity width, ω_v (equivalent Gaussian width), of the MgII $\lambda 2796$ transition as a function of absorption redshift. The dotted line gives the limit for unresolved absorption features. The data points with “rings” are those systems that have multiple absorption features separated by continuum. The open data point (with ring) is measured from the $\lambda 2803$ transition because the $\lambda 2796$ transition was unavailable. There is no evidence for any trend in ω_v with redshift.

seven systems in which MgI is detected, three have $W_r(2796) \leq 0.11 \text{ \AA}$. Two of the MgI “clouds” are in multiple component systems, S10 and S29, and these clouds have $W_r(2796) = 0.11 \text{ \AA}$ and 0.05 \AA , respectively. There does not appear to be a clear threshold for the presence of MgI with the equivalent width of MgII down to $W_r(2796) \sim 0.1 \text{ \AA}$. It appears that MgI can survive in sub-LLS environments.

In Figure 10, we present $W_r(1548)$ versus $W_r(2796)$ from the data presented in Table 4. Included in this table are the number of absorption components (not VP components) seen in MgII absorption, and $W_r(2796)$, $W_r(2600)$, and $W_r(1548)$. Upper limits are denoted with downward arrows. A tentatively suggested ionization condition, either L (low), H (high), or M (multi-phase), is given. Filled circles are those designated as L or M, open circles as H, and boxes as undetermined ionization conditions. We elaborate on these inferred conditions in §5.2, where the terms L, H, and M are defined and photoionization models are presented.

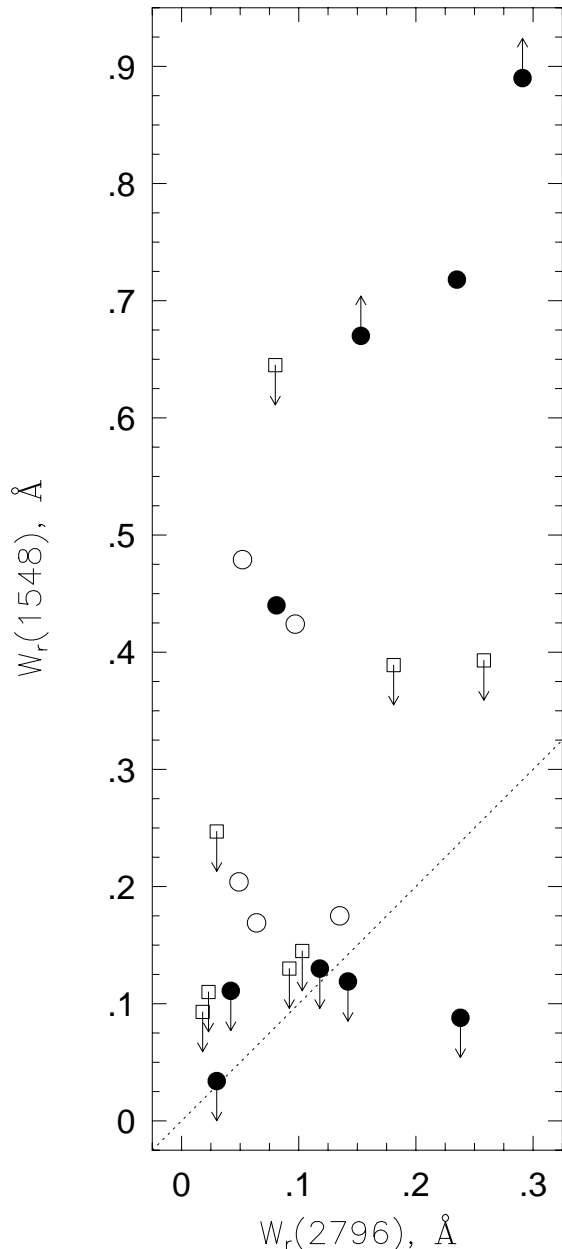


Fig. 10.— $W_r(1548)$ versus $W_r(2796)$. Based upon photoionization models, the data are designated as low or multi-phase ionization conditions (solid circles), high ionization (open circles), or undetermined (open boxes). See text for definitions. Downward arrows give upper limits on $W_r(1548)$. The two upward arrows are lower limits for an assumed optically thick doublet ratio in unresolved optical data taken from the literature. The dotted line is $W_r(1548) = W_r(2796)$.

In summary, we find that a typical individual MgII absorbing cloud is characterized by $W_r(2796) \leq 0.15 \text{ \AA}$, and a temperature of $\sim 25,000 \text{ K}$. The presence or non-presence of MgI does not appear have a threshold dependence upon $W_r(2796)$ down to 0.1 \AA , and the ionization conditions appear to cover a broad range as inferred from the equivalent width ratios of CIV, FeII and MgII.

5. On the Nature of Weak MgII Absorbers

5.1. Comparison with Lyman Limit Systems

A corresponding Lyman limit break is almost always found in UV spectra at the redshift of a strong MgII absorber (Lanzetta 1988). Thus, the majority of strong MgII absorbers are believed to arise in LLS environments. We are led to conclude that *virtually all weak MgII absorbers arise in sub-LLS environments*, as can be inferred directly from Figure 5 (right hand panel). The dN/dz of $W_r^{\min}(2796) = 0.3 \text{ \AA}$ MgII absorbers and of LLS absorbers are consistent within uncertainties, with the number density of the strong MgII absorbers being slightly higher (SS92; Stengler-Larrea et al. 1995). However, for the $W_r^{\min}(2796) = 0.02 \text{ \AA}$ MgII absorbers (combined sample of this work and SS92), $dN/dz = 2.65$, which is a factor of 3.8 ± 1.1 greater than that of the strong MgII-LLS absorbers.

That weak MgII systems arise in sub-LLS environments is also consistent with the expectations for photoionized clouds. From preliminary Voigt profile fits, we have found $10^{11.8} \leq N(\text{MgII}) \leq 10^{13.2} \text{ cm}^{-2}$ for the individual clouds. We built a grid of photoionization models using CLOUDY (Ferland 1996), where we have assumed a Haardt & Madau (1996) extra-galactic UV background spectrum normalized at $z = 1$ and a solar abundance pattern with $[Z/Z_\odot] = -1$ (which can be interpreted as the “gas-phase metallicity”, accounting for possible dust depletion of MgII). The model clouds are constant density plane-parallel slabs, each defined by its neutral hydrogen column density, $N(\text{HI})$, and ionization parameter, $U = n_\gamma/n_{\text{H}}$, where n_γ and n_{H} are the number density of photons capable of ionizing hydrogen and the total hydrogen number density, respectively.

In Figure 11, the grid of clouds is plotted for $N(\text{MgII})$ versus the total hydrogen column density, $N(\text{HI}) + N(\text{HII})$. Solid curves are lines of constant $N(\text{HI})$, and dotted curves are lines of constant $\log U$ presented at intervals of 0.5 dex. The range of observed weak MgII absorber column densities is

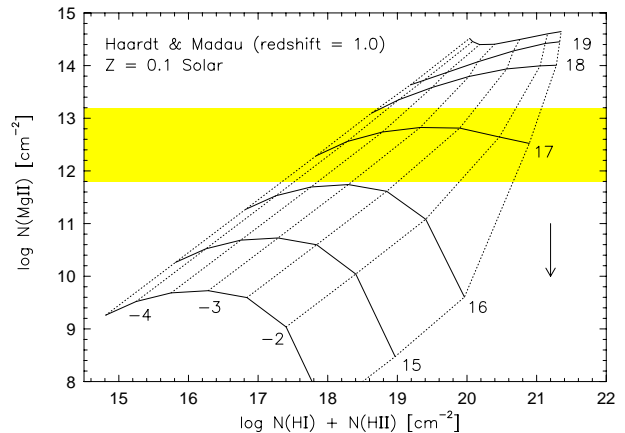


Fig. 11.— MgII column density versus total hydrogen column density for a grid of CLOUDY photoionization models, assuming a Haardt & Madau (1996) UV flux at $z = 1$. A $Z = 0.1Z_\odot$ abundance pattern has been assumed. The solid curves are contours of constant $N(\text{HI})$ and the dot-dot curves are contours of constant ionization parameter, $\log U$. The shaded region gives the locus of measured $N(\text{MgII})$ for the sample, based upon Voigt profile fits to the data (Paper II). For this abundance pattern, clouds which have $N(\text{FeII})/N(\text{MgII}) \sim 1$ must have low ionization, $\log U \sim -3.5$. The arrow shows how the grid would move if the metallicity of the models were decreased by 1 dex.

crudely represented by the shaded region. Note that the majority of the absorbers are predicted to arise in sub-LLS clouds, those with $N(\text{HI}) \leq 10^{17.3} \text{ cm}^{-2}$. A main point to be gleaned from Figure 11, however, arises due to the metallicity dependence of the photoionization grid. If the metallicity of the model clouds were reduced by 1 dex, the entire grid would move approximately 1 dex downward along the $N(\text{MgII})$ axis. Thus, if the metallicity of the clouds were much lower than $[Z/Z_\odot] = -1$, the majority of the inferred neutral hydrogen column densities would lie above the Lyman limit value of $10^{17.3} \text{ cm}^{-2}$. This is not allowed because most all weak MgII absorbers must arise in sub-LLS environments as constrained by the dN/dz of LLS absorbers. Our inferred upper limit on the metallicity would scale roughly in direct inverse proportion to any α -group abundance enhancement.

In conclusion, if the weak MgII absorbers are pho-

toionized by a Haardt & Madau-like spectrum, then the cloud metallicities are (1) $[Z/Z_{\odot}] \geq -1$ with $[\alpha/\text{Fe}] \sim [\alpha/\text{Fe}]_{\odot}$, or (2) $[Z/Z_{\odot}]$ slightly below -1 with $[\alpha/\text{Fe}] > [\alpha/\text{Fe}]_{\odot}$ by a factor of a few. Such abundance patterns are consistent with those observed in the Galaxy (Lauroesch et al. 1996; Savage & Sembach 1996). The metallicity cannot typically be significantly lower than $[Z/Z_{\odot}] = -1$, since that would require an implausibly large enhancement of $[\alpha/\text{Fe}]$ with respect to the solar ratio.

5.2. Comparison with CIV Systems: Ionization Conditions

Sargent, Boksenberg, & Steidel (1988) found $dN/dz = 1.76 \pm 0.33$ for CIV at $\langle z \rangle = 1.5$ for a sample complete to $W_r^{\text{min}}(1548) = 0.3 \text{ \AA}$. We note that this value is consistent with the number per unit redshift of the weak MgII systems at $\langle z \rangle = 0.9$. Does this imply that the population of systems selected by weak MgII absorption are, in essence, the same population as selected by the presence of CIV with $W_r^{\text{min}}(1548) = 0.3 \text{ \AA}$? It is not expected that all weak MgII systems at $\langle z \rangle = 0.9$ would have associated CIV with $W_r(1548) \geq 0.3 \text{ \AA}$, since the CIV number density is seen to decrease with decreasing redshift for this equivalent width threshold. Bergeron et al. (1994) found $dN/dz = 0.87 \pm 0.43$ for CIV with $W_r^{\text{min}}(1548) = 0.3 \text{ \AA}$ at $\langle z \rangle = 0.3$. We have confirmed this expectation with our search for CIV in FOS/*HST* spectra. Of the 13 systems for which CIV was not detected in FOS/*HST* spectra, all but three have a 3σ $W_r(1548)$ threshold below 0.3 \AA . Of course, weaker CIV could always be present.

In and of itself, CIV absorption is an important indicator of the ionization level in absorbers selected by weak MgII absorption. A more powerful indicator, however, is the relative absorption strengths of CIV and FeII. In the upper panels (a and b) of Figure 12, we present the column densities of MgII, FeII, MgI, AlIII, and CIV as a function of ionization parameter for CLOUDY (Ferland 1996) models. We have assumed $N(\text{HI}) = 10^{16.5} \text{ cm}^{-2}$ for two metallicities, $[Z/Z_{\odot}] = -1$ and 0 , respectively, with a Haardt & Madau (1996) UV background flux normalized at $z = 1$. The bottom panels (c and d) show the rest-frame equivalent widths for a Doppler parameter of $b = 6 \text{ km s}^{-1}$, the median velocity width of the *individual* MgII absorption components¹². The models

presented have MgII $\lambda 2796$ equivalent widths consistent with the observed range for individual components (see Figure 8). For these sub-LLS clouds, the models show no temperature or ionization structure with cloud depth; the kinetic temperature is the same for all ionization species. For the modeled column densities, MgI $\lambda 2853$, FeII $\lambda 2600$, and AlIII $\lambda 1855$ are on the linear part of the curve of growth (b independent). For MgII $\lambda 2796$ and CIV $\lambda 1548$, the value of the b parameter becomes important for column densities greater than $\sim 10^{11} \text{ cm}^{-2}$ and $\sim 10^{13} \text{ cm}^{-2}$, respectively. We have neglected thermal scaling of the b parameters, which would yield slightly elevated CIV equivalent widths.

The demarcation between low and high ionization absorbers (L and H, respectively, as marked on panels c and d of Figure 12) is given by the ratio $W_r(1548)/W_r(2796)$, where greater than unity designates high ionization (Bergeron et al. 1994). For these single-phase photoionization models, high ionization clouds have $N(\text{FeII}) \ll N(\text{MgII})$ and $N(\text{FeII}) \ll N(\text{CIV})$. For low ionization gas there is a range of $N(\text{FeII})$ as compared to $N(\text{CIV})$ and $N(\text{MgII})$. For very low ionization conditions, $N(\text{FeII})$ can be comparable to $N(\text{MgII})$, with both much larger than $N(\text{CIV})$. We would not expect CIV to be reported in the literature nor found in FOS/*HST* spectra for clouds with $W_r(2600)/W_r(2796) > 0.1$ (roughly). In fact, for no case in which we have detected FeII would we expect a high-ionization single-phase cloud as defined by $W_r(1548)/W_r(2796) \geq 1$. The point is that the presence of FeII absorption at a non-negligible level is a strong indicator of low ionization conditions for single-phase clouds. The above arguments remain valid for $N(\text{HI}) = 10^{17} \text{ cm}^{-2}$ cloud models in which some ionization structure is present, resulting in roughly constant $N(\text{MgII})$ as a function of $\log U$, but identical behavior in $N(\text{FeII})$ and $N(\text{CIV})$.

As seen in Table 4, of the 22 systems for which both CIV and FeII was available, four have FeII but no CIV (S7, S10, S18, and S22). These are low ionization systems. Five of 22 systems have CIV but no FeII (S5, S17, S19, S20, and S23) to $\langle W_r^{\text{min}}(2600) \rangle \sim 0.01 \text{ \AA}$; these may be high ionization systems. Four of 22 systems have both CIV and FeII (S14, S28, S29, and S30), two of which (S28 and S29) also have MgI. *The*

ample, S2, S4, S5, S21, S23) reveals that they are blends of narrower components. Preliminary Voigt Profile decomposition of the profiles is consistent with $b = 6 \text{ km s}^{-1}$ clouds.

¹²Inspection of the MgII profiles with $\omega_v \geq 10 \text{ km s}^{-1}$ (for ex-

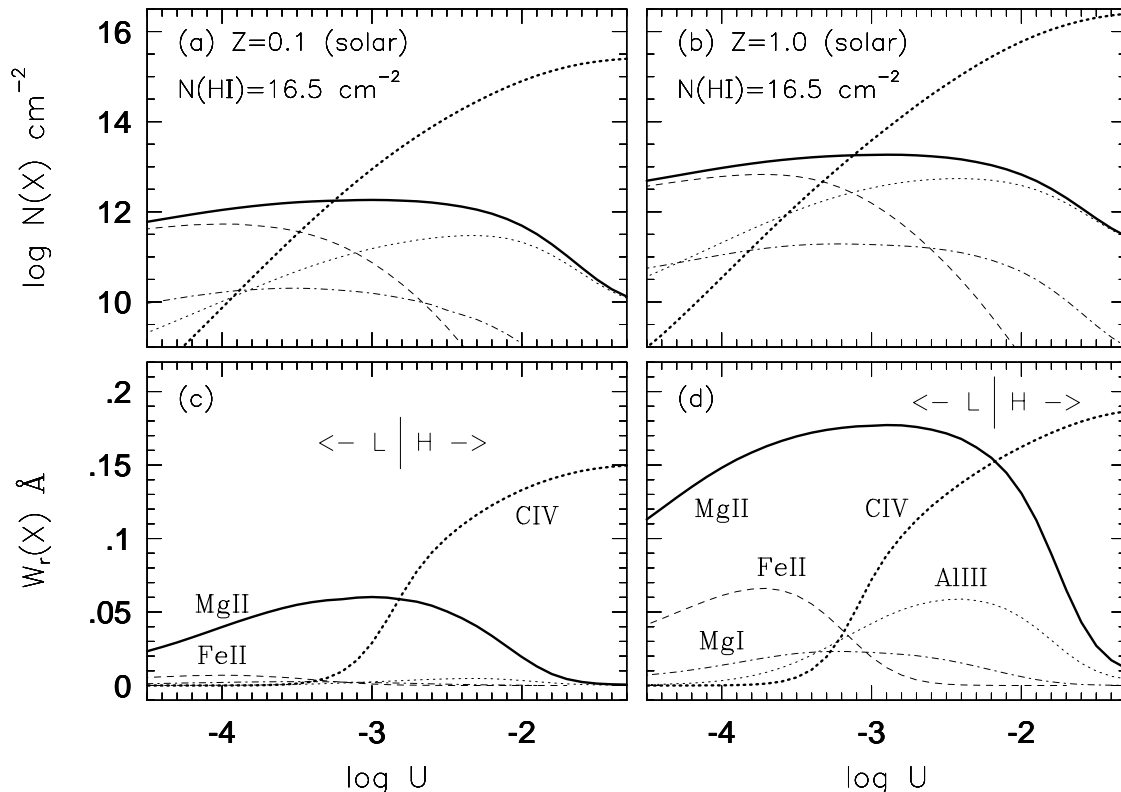


Fig. 12.— Photoionization models with $N(\text{HI}) = 10^{16.5} \text{ cm}^{-2}$ for solar abundance patterns with $[Z/Z_{\odot}] = -1$ (left panels) and $[Z/Z_{\odot}] = 0$ (right panels). The upper panels show the observed column densities as a function of ionization parameter and the lower panels show the rest-frame equivalent widths for $b = 6 \text{ km s}^{-1}$ for CIV $\lambda 1548$, MgII $\lambda 2796$, FeII $\lambda 2600$, MgI $\lambda 2853$, and AlIII $\lambda 1855$. Low and high ionization (“L” and “H”, respectively) are defined by the ratio of $W(\text{CIV})/W(\text{MgII})$.

simultaneous presence of FeII and CIV implies that a single cloud or a single-phase absorption model is not adequate. From this, we speculate that S11, S13, and S26 are either low or multi-phase systems due to their having substantial FeII, even though we have no information on CIV. Overall, it appears that the population of metal-line absorbers selected by weak MgII absorption have a range of ionization conditions, possibly including multi-phase conditions. In Figure 10, we have illustrated these suggested ionization conditions.

5.3. Evidence for Multi-Phase Ionization

From Figure 12, we see that it is difficult to obtain $W_r(1548) > 0.2 \text{ \AA}$ for single-phase photoionization models with profile widths (i.e. b parameters) consistent with those observed for individual MgII components. This is because of the very flat dependence of $W_r(1548)$ on $N(\text{CIV})$ for the small b pa-

rameters implied by the individual MgII components. This upper limit holds for higher $N(\text{HI})$ cloud models. The upshot is that if $W_r(1548)$ is significantly greater than $\sim 0.2 \text{ \AA}$ in a single component absorber with $W_r(2796) \leq 0.2 \text{ \AA}$, one of two possibilities can be inferred: (1) Either the absorber has multiple ionization phases, such that the MgII arises in a cooler low-ionization region embedded in a higher ionization medium, or (2) additional multiple components (spatially distinct) are observed in CIV but not in MgII, in which case a high resolution spectrum of the CIV profile would be required to determine the ionization level of the components seen in MgII.

Three of the four systems exhibiting both CIV and FeII absorption, S14, S29, and S30, have multiple unblended components spread over $\sim 100 \text{ km s}^{-1}$. It is quite plausible that they are multi-phase, that low ionization MgII components are embedded in a high ionization “halo”. Consider S29, which has six components. We estimated $W_r(1548) \simeq 0.9 \text{ \AA}$ (lower

limit) from the unresolved CIV equivalent width reported by SS92. For $N(\text{HI}) \leq 10^{17} \text{ cm}^{-2}$, the CIV equivalent width could be produced as the component sum of high ionization clouds (near-solar metallicity required), each component contributing $\sim 0.2 \text{ \AA}$ to the total CIV equivalent width. However, this is unlikely because the FeII absorption enforces low ionization conditions in the phase giving rise to MgII absorption. The mean equivalent width of the individual MgII $\lambda 2796$ components is 0.05 \AA and that of FeII $\lambda 2600$ is 0.015 \AA . Referring to Figure 12, the mean ratio of $W_r(2600)/W_r(2796) \simeq 0.3$ for $W_r(2796) \simeq 0.05 \text{ \AA}$ implies ionization parameters in the range $-3.5 \leq \log U \leq -4$; these are low ionization clouds. Thus, the overall absorption properties of S29 are more consistent with low ionization MgII components embedded in a high ionization medium or juxtaposed with additional spatially distinct high ionization components.

5.4. The Physical Sizes of the Absorbers

The measured dN/dz can be used to constrain their physical sizes, assuming that all absorbers are associated with luminous galaxies (Steidel 1995; Churchill et al. 1996). For a Schechter function (1976), $\Phi(L)dL = \Phi^* (L/L^*)^\alpha \exp(-L/L^*) dL$, there are two important parameters: the faint-end slope, α , and the density of L^* galaxies, Φ^* . Second, a Holmberg (1975) dependence, $R(L) = R^* (L/L^*)^\beta$, of the spatial extent of the absorbing gas on the luminosity of the galaxy is assumed, where R^* is the fiducial size of an L^* galaxy. The product σn , is given by $\sigma n = \pi \int_{L_{\min}}^{\infty} \Phi(L) R^2(L) dL$, which simplifies to

$$\sigma n = \pi \Phi^* R^{*2} \Gamma(\alpha + 2\beta + 1, L_{\min}/L^*), \quad (8)$$

where Γ is the incomplete gamma function, which accounts for the additional assumption of a minimum luminosity, L_{\min} , at which a galaxy will no longer exhibit MgII absorption to a well-defined detection level at any impact parameter. Assuming no evolution in the redshift path density of absorbing galaxies, the relation between σn and the measured dN/dz is

$$\frac{dN}{dz} = \frac{c\sigma n}{H_0} (1+z)(1+2q_0z)^{-1/2}. \quad (9)$$

For $W_r^{\min}(2796) = 0.3 \text{ \AA}$, Steidel (1995) directly measured $\beta = 0.15$ and $R^* = 38h^{-1} \text{ kpc}$ for the Holmberg relation and $L_{\min}/L^* \sim 0.06$ for K -band

luminosities. From this, Steidel et al. (1994) deduced a faint-end slope of $\alpha = -1$ and a number density of $\Phi^* = 0.03h^3 \text{ Mpc}^{-3}$ for galaxies selected by the presence of MgII absorption. These values are in good agreement with the values $\alpha = -0.9$ and $\Phi^* = 0.033h^3 \text{ Mpc}^{-3}$ measured for the Canada-France Redshift Survey (CFRS) sample of galaxies over the similar redshift range of $0.0 \leq z \leq 1.3$ (Lilly et al. 1995). However, it is not entirely clear that the radius-luminosity relationship measured by Steidel (1995) is applicable when the equivalent width detection threshold is lowered to $W_r^{\min}(2796) = 0.02 \text{ \AA}$. Nor is there *a priori* reason to assume that the $L_{\min}/L_K^* = 0.06$ cut off should apply for a population of galaxies selected by $W_r(2796) < 0.3 \text{ \AA}$ absorption. It is possible that low surface brightness (LSB) galaxies contribute to the measured dN/dz of weak MgII absorbers¹³ (Impey & Bothun 1989; Churchill & Le Brun 1998). At redshift $z \sim 0$, Dalcanton et al. (1997) has measured $\Phi^* = 0.08h^3 \text{ Mpc}^{-3}$ for LSB galaxies with central surface brightnesses of $23 \leq \mu_0(V) \leq 25 \text{ mag arcsec}^{-2}$. This is a factor of ~ 2.5 higher than the number density of CFRS and MgII-selected galaxies, which exhibit the Freeman (1970) central surface brightness of $\mu_0(B) = 21.7 \text{ mag arcsec}^{-2}$. Thus, we do not simply assume that the luminosity function of galaxies selected by weak MgII absorption would have the same number density as that found by Steidel et al. (1994) for strong systems.

For $W_r^{\min}(2796) = 0.02 \text{ \AA}$, we found $dN/dz = 2.71$ at $\langle z \rangle = 0.9$. Writing Eq. 8 to obtain R^* as a function of Φ^* , L_{\min}/L^* , and β , gives,

$$R^* = 79.5h^{-1} \left[\left(\frac{\Phi^*}{\Phi_{\text{CFRS}}^*} \right) \Gamma(2\beta, L_{\min}/L^*) \right]^{-1/2} \text{ kpc}, \quad (10)$$

where it is assumed that the absorbing gas is spherically distributed and has unity covering factor¹⁴. For $L_{\min}/L^* = 0.06$, $\beta = 0.15$, and $\Phi^*/\Phi_{\text{CFRS}}^* \sim 1$, the inferred R^* is $63h^{-1} \text{ kpc}$. If LSB galaxies have the same absorbing properties as do those observed by Steidel (1995), then the combined galaxy population

¹³We comment that it is interesting that LSB galaxies have not yet been identified with strong MgII absorption, except possibly in the cases of a few damped Ly α systems.

¹⁴If one assumes that only some fraction, f_{abs} , of the galaxies contribute to absorption, and that the gas covering factor, f_c , is less than unity, then the quoted values of R^* should be scaled by $(f_{\text{abs}}f_c)^{-1/2}$. If one assumes the geometry is somewhat flattened, then an additional factor of $\kappa^{-1/2}$ can be introduced, where $\kappa = 0.5$ for infinitely thin “disks”.

would have $\Phi^*/\Phi_{\text{CFRS}}^* \sim 3$ (Dalcanton et al. 1997), which yields $R^* \sim 35h^{-1}$ kpc. This is surprisingly consistent with the R^* measured by Steidel (1995) for $W_r(2796) > 0.3 \text{ \AA}$ absorption selected galaxies. For $L_{\text{min}}/L^* = 0$, $\beta = 0.15$, and $\Phi^*/\Phi_{\text{CFRS}}^* \sim 1$, the inferred size is $R^* = 46h^{-1}$ kpc. If $\beta \sim 0$ with $L_{\text{min}}/L^* = 0.06$, then $R^* = 53h^{-1}$ kpc. If $\beta = 0.4$ (the historically invoked ‘‘Holmberg’’ value), then $R^* = 77h^{-1}$ kpc.

5.5. Evolution of $n(W_r)$

If the absorbing gas is photoionized by the extra-galactic UV background, then ionization conditions are expected to be higher at higher redshifts. In fact, Bergeron et al. (1994) have found that the ratio of ‘‘high’’ to ‘‘low’’ ionization metal-line absorbers increases with increasing redshift at a rate that is not inconsistent with a factor of ~ 5 increase in the UV background (Kulkarni & Fall 1993). Our observations place no constraint on the evolution of the weak MgII absorbers over this redshift range.

In principle, it might be that at $z \sim 2$ the MgII equivalent width distribution exhibits a cut off at the smallest equivalent widths. It is also expected that the power-law slope of the distribution is flatter for larger equivalent widths at $z \sim 2$ [there are more large $W_r(2796)$ absorbers at high redshift] than that measured in this work at $z \sim 1$. This implies a very curious effect in the inferred evolution of MgII absorption strengths as the minimum equivalent width of the sample covering $0.4 \leq z \leq 2.2$ is continually decreased. It is well established that for $W_r^{\text{min}}(2796) = 0.3 \text{ \AA}$, the population is consistent with no-evolution expectations, and that the lack of evolution is dominated by the lower end of the equivalent width distribution to this $W_r^{\text{min}}(2796)$. When $W_r^{\text{min}}(2796)$ is increased, the evolution becomes pronounced in that the ratio of ‘‘large’’ to ‘‘small’’ $W_r(2796)$ absorbers increases with increasing redshift (SS92). Since the UV background is more intense at higher redshifts, one would expect that the presence of MgII is increasingly dependent upon photon shielding by neutral hydrogen; at $z \sim 2$ (and above), it would be expected that MgII would not survive in sub-LLS environments (also see discussion in §7 of SS92). Therefore, as $W_r^{\text{min}}(2796)$ is decreased from 0.3 \AA to $\sim 0.02 \text{ \AA}$ for a $0.4 \leq z \leq 2.2$ sample, *evolution should again become apparent, this time due to a paucity of weak systems at the higher redshifts*. This trend is tentatively suggested by the fact that at $\langle z \rangle = 0.9$ there is a 30%

difference between the dN/dz of $W_r^{\text{min}}(2796) = 0.3 \text{ \AA}$ absorbers and LLS absorbers, whereas there is only an 8% difference at $\langle z \rangle = 2$ (SS92; Stengler-Larrea et al. 1995).

6. Summary

We searched for weak MgII $\lambda\lambda 2796, 2803$ doublets, those with rest-frame equivalent widths $W_r(2796) < 0.3 \text{ \AA}$, in HIRES/Keck spectra of 26 QSOs. The QSO sight lines are unbiased for these weak systems. The cumulative redshift path was $Z \sim 17$ over the range $0.4 \leq z \leq 1.4$ and $Z \sim 0.7$ for $1.4 \leq z \leq 1.7$. The survey was complete to $W_r(2796) = 0.06 \text{ \AA}$, and 80% complete to $W_r(2796) = 0.02 \text{ \AA}$, where we have enforced a 5σ detection limit. A total of 30 systems were detected, of which 23 were discovered in these spectra. The MgI $\lambda 2853$ transition was detected in seven of the systems and FeII, especially the $\lambda 2600$ and/or the $\lambda 2383$ transition, was detected in half of the systems. When AlIII $\lambda\lambda 1855, 1863$ was covered, we found it in three of four systems. From a literature search and a search we conducted in archival FOS/HST spectra, we detected CIV in nine of 22 covered systems to 3σ equivalent width threshold of 0.03 to 0.3 \AA (rest-frame). No systems were found at $1.4 \leq z \leq 1.7$, though this is consistent with expectations when we extrapolate from lower z , given that the cumulative redshift path was only $Z \sim 0.7$ over this redshift range. We have combined our sample with the $W_r(2796) \geq 0.3 \text{ \AA}$ sample MG1 of SS92, taken over the redshift interval $0.4 \leq z \leq 1.4$, and measured the redshift number density and equivalent width distribution of MgII absorbers with $W_r(2796) \geq 0.02 \text{ \AA}$.

Main results from this work include:

1. The redshift path density of weak MgII absorbers was measured to be $dN/dz = 1.74 \pm 0.11$. There is no evidence for evolution in the redshift path density, but the measured value of $\gamma = 1.3 \pm 0.9$ is not constraining. Incorporating the MG1 sample of SS92 [$W_r^{\text{min}}(2796) = 0.3 \text{ \AA}$], we find that the *total* number density per unit redshift for systems with $W_r^{\text{min}}(2796) = 0.02 \text{ \AA}$ at $\langle z \rangle = 0.9$ is $dN/dz = 2.65 \pm 0.15$. The dN/dz of weak MgII absorbers is roughly 5–7% of that of the Ly α forest with $W_r(\text{Ly}\alpha) \geq 0.1 \text{ \AA}$ (Jannuzi et al. 1998). Thus, it is plausible that $\sim 5\%$ of $z \sim 0.9$ ‘‘Ly α clouds’’ will have detectable MgII absorption to $W_r(2796) = 0.02 \text{ \AA}$.

2. For $W_r^{\min}(2796) = 0.02 \text{ \AA}$, MgII absorbers at $\langle z \rangle = 0.9$ outnumber LLS absorbers by a factor of 3.8 ± 1.1 . That the populations of strong MgII absorbers and LLS are indistinguishable (Lanzetta 1988) strongly suggests that virtually all of the weak MgII systems arise in sub-LLS environments. It is possible that the weak MgII systems have high metallicities, whether their ionization conditions are low or high (see Figures 11 and 12). Photoionization models, using Ferland’s CLOUDY, are consistent with this conclusion; many weak MgII absorbers probably have $[Z/Z_\odot] \geq -1$. Lower metallicities require $N(\text{HI})$ above the Lyman limit value, which is not allowed because the ratio of dN/dz of weak MgII absorbers to that of LLS absorbers requires that most all weak MgII absorbers have $N(\text{HI})$ near or below the Lyman limit value.
3. The equivalent width distribution was found to follow a power law with slope $\delta \sim 1.0$ down to $W_r(2796) = 0.017 \text{ \AA}$. *There is no turnover or break in the equivalent width distribution for $W_r(2706) < 0.3 \text{ \AA}$ at $\langle z \rangle = 0.9$.* A single power-law slope does not describe the equivalent width distribution over the full redshift range $0.3 \leq z \leq 2.2$. For $z < 1.4$, there is a break (a significantly steeper slope) in the distribution for $W_r(2796) > 1.3 \text{ \AA}$. The upper limit on this slope is $\delta = 2.3$.
4. Most, if not all, of the *individual clouds* in these weak absorbers have $W_r(2796) \leq 0.15 \text{ \AA}$. Their line widths are narrow, with an average of $\sim 4 \text{ km s}^{-1}$, implying temperatures of $\sim 25,000 \text{ K}$. The presence of MgI is not correlated with $W_r(2796)$ or with the MgII doublet ratio. In fact, MgI absorption is present in at least one component having $W_r(2796)$ as small as 0.08 \AA . Statistically, there appears to be no $W_r(2796)$ threshold for the presence of MgI down to $W_r(2796) \sim 0.1 \text{ \AA}$.
5. The weak MgII absorbers may comprise a diverse population, including low, high, and multi-phase ionization systems. The low ionization systems would be immediately recognizable by the presence of $W_r(2600)/W_r(2796) \geq 0.1$. In a single MgII component with $b \leq 6 \text{ km s}^{-1}$ and $W_r(2796) < 0.2 \text{ \AA}$, the presence of CIV with $W_r(1548) \geq 0.2 \text{ \AA}$, and especially the simultaneous presence of FeII and CIV, may be due to

multi-phase absorption or additional spatially distinct high ionization components in which MgII has not been detected. In an absorber with N_c components in which the individual components have $b \leq 6 \text{ km s}^{-1}$ and $W_r(2796) < 0.2 \text{ \AA}$, multi-phase or additional high ionization components are likely if the total system CIV equivalent width is larger than $\sim N_c \times 0.2 \text{ \AA}$. Again, this is especially true if the individual MgII components have $W_r(2600)/W_r(2796) \geq 0.1$.

6. The velocity clustering of weak MgII absorbers around strong ones is consistent with a random distribution; a χ^2 test yielded a probability of 0.18 that clustering was drawn from a random distribution. Furthermore, we examined the redshift clustering of the weak systems with respect to one another and found that the systems are also not inconsistent with a random distribution. The χ^2 probability was 0.25. We conclude that the QSO sight lines surveyed for this work are unbiased for the presence of weak MgII absorbers.
7. Assuming the radius-luminosity relationship between gas and galaxies and the cut off, L_{\min} , in the MgII absorbing galaxy luminosity function (Steidel 1995), we inferred an R^* for $W_r^{\min}(2796) = 0.02 \text{ \AA}$ MgII absorbers of $65h^{-1} \text{ kpc}$. If there is no radius-luminosity dependence, then $R^* \simeq 55h^{-1} \text{ kpc}$. If there is no luminosity cut off, then $R^* \simeq 45h^{-1} \text{ kpc}$. If LSB galaxies have the same absorbing properties as do the MgII selected galaxies observed by Steidel (1995), then the combined galaxy population would have $R^* \sim 35h^{-1} \text{ kpc}$. It is not inconsistent with the data to suggest that a non-negligible fraction of the weak MgII absorbers are arising in LSB galaxies.

6.1. Objects Selected by Weak MgII Absorption

The question remains; what luminous objects could be associated with the large numbers of weak MgII systems at $0.4 \leq z \leq 1.4$? Do the galaxies selected by MgII absorption with $W_r(2796) \geq 0.3 \text{ \AA}$ (Steidel 1995; Steidel et al. 1994) tell the whole story or do they represent the “tip of the MgII iceberg”. Are weak MgII absorbers analogous to a bulk of material that lies hidden below the “galactic water line”? That is,

are a substantial fraction not directly associated with bright galaxies, but rather with intergalactic material or “failed” galaxies? Given that only four of 20 have obvious galaxy counterparts, it is not clear that the surface brightnesses of the star forming environments associated with weak MgII absorbers are above the Freeman (1970) value. It could be that the successful broad-band imaging technique for identifying the luminous counterparts of strong MgII absorbers in QSO fields will be less effective for locating many of the counterparts associated with weak MgII absorbers.

If weak MgII absorption arises in the extended regions of MgII absorption-selected galaxies, it likely is most often occurring at large impact parameters (a region of $D \geq 40h^{-1}$ kpc; beyond the well probed regions within $10''$ of the QSO). It is possible that some fraction of the Ly α lines seen to arise beyond ~ 40 kpc of large extended halos or disks of galaxies (Lanzetta et al. 1995; Le Brun, Bergeron, & Boissé 1996) give rise to weak MgII absorption. An alternative possibility is that some fraction of the weak MgII population is selecting sub-LLS environments around LSB galaxies or low luminosity galaxies, those with $L_K < 0.06K_K^*$. That is, some fraction of weak systems could arise in “normal” high surface brightness galaxies (perhaps at greater impact parameters) and some fraction could arise in dwarf or large LSB galaxies.

Conceivably, LSB galaxies could significantly contribute to the weak MgII absorption cross section. At the low redshifts studied in this work, most sub-LLS absorbers are thought to be associated with LSB galaxies (Salpeter 1993; Linder 1997). Impey & Bothun (1989), upon reexamining the selection effects and assumptions that go into the calculations of galaxy cross sections from QSO absorbers, found that LSB galaxies are expected to dominate the absorption cross section. If so, why would it be that strong MgII absorbers are not associated with LSB galaxies more often than or as often as are normal bright galaxies? And, when strong MgII absorption is associated with an LSB galaxy, why is it that the absorbers are damped Ly α systems (Steidel et al. 1994; Le Brun et al. 1997)? LSB galaxies typically have HI surface densities a factor of two lower than normal high surface brightness galaxies (de Blok, McGaugh, & van der Hulst 1996) and lower metallicities (McGaugh 1994). Further, the inner $15h^{-1}$ kpc of LSB galaxies are found to have $N(\text{HI})$ of a few $\times 10^{20}$ cm $^{-2}$ (de Blok et al. 1996), i.e. they are damped Ly α

absorbers. It could be that some weak MgII absorbers arise in LSB galaxies at galactocentric distances greater than $\sim 15h^{-1}$ kpc, where the HI environment is sub-Lyman limit and clouds cannot have large MgII column densities. Thus, it is possible that the strong MgII (and FeII) associated with damped Ly α absorbers in LSB galaxies arise in their inner regions, whereas only weak MgII absorbing clouds can survive in their outer regions.

Other possibilities include isolated star forming or post star forming dwarf galaxies and/or pre-galaxy fragments (Yanny & York 1992), or the remnant material left over from the formation of galaxies and/or small galaxy groups (Bowen et al. 1995; van Gorkom et al. 1996; Le Brun et al. 1996). Narrow band imaging of emission lines at the absorber redshifts might provide a test for the former scenario, while charting the distribution of galaxies at the absorber redshifts in wide fields ($\sim 100''$) centered on the QSOs might provide tests for the latter. A more detailed determination of the chemical and ionization conditions and identification of the luminous objects associated selected by weak MgII absorption is the next logical step toward their further exploration.

This work has been supported in part by the National Science Foundation Grants AST-9617185 and AST-9529242, by NASA LTSA grant NAG5-6399, and by a Sigma-Xi Grant in Aid of Research. CWC acknowledges support as a Eberly School of Science Distinguished Postdoctoral Fellowship. We especially thank Sofia Kirhakos, Buell Jannuzi, and Don Schneider for permission to publish results from our CIV search using the archival FOS/*HST* from our collaboration. Thanks are extended to Adam Dobrzycki for kindly assisting us with a preliminary search for CIV through his FOS/*HST* archival spectra. Thanks to G. Ferland for making CLOUDY a public tool. We thank an anonymous referee and the scientific editor for comments that led to an improved manuscript. This paper is dedicated to the life of Julius L. Nelson.

REFERENCES

- Bahcall, J. N., et al. 1996, ApJ, 457, 19 (KP VII)
- Bergeron, J. et al. 1994, ApJ, 436, 33
- Bergeron, J., and Boissé, P. 1991, A&A, 243, 344
- Bowen, D. V., Blades, J. C., Pettini, M. 1995, ApJ, 448, 634
- Calet, A. 1989, ApJ, 340, 90
- Churchill, C. W. 1995, Lick Observatory Technical Report, #74
- Churchill, C. W. 1997a, Ph. D. Thesis, University of California, Santa Cruz
- Churchill, C. W., Charlton, J. C., Rigby, J. R., Januzzi, B. T., Kirhakos, S., and Vogt, S. S. 1998, in progress (Paper II)
- Churchill, C. W., and Charlton, J. C. 1998, ApJ, submitted
- Churchill, C. W., and Le Brun, V. 1998, ApJ, 499, 677
- Churchill, C. W., Steidel, C. C., and Vogt, S. S. 1996, ApJ, 471, 164
- Churchill, C. W., Vogt, S. S., and Charlton, J. C. 1998, ApJS, to be submitted (CVC98)
- Dalcanton, J. J., Spergel, D. N., Gunn, J. E., Smith, M., and Schneider, D. P. 1997, AJ, 114, 635
- Dobrzycki, A., Bechtold, A., Wilden, B., Morita, M., Dobrzycka, D., Scott, J., Tran, K-V. 1998, ApJ, in preparation
- de Blok, W. J. G., McGaugh, S. S., and van der Hulst, J. M. 1996, MNRAS, 283, 18
- Ferland, G. 1996, Hazy, University of Kentucky Internal Report
- Freeman, K. 1970, ApJ, 160, 811
- Haardt, F., and Madau, P. 1996, ApJ, 461, 20
- Holmberg, E. 1975, in Galaxies and the Universe, ed. A. Sandage, M. Sandage, & J. Christian (Chicago: University of Chicago Press), 123
- Impey, C., and Bothun, G. 1989, ApJ, 341, 89
- Impey, C., Petry, C. E., Malkan, M. A., and Webb, W. 1996, ApJ, 463, 473
- Jannuzi, B. T., et al., 1998, in press (KP XIII)
- Kirhakos, S., et al. 1992, PASP 646, 1994
- Kulkarni, V. P., and Fall, S. M. 1994, ApJ, 413, L63
- Lanzetta, K. M., Turnshek, D. A., and Wolfe, A. M. 1987, ApJ, 322, 739 (LTW)
- Lanzetta, K. M. 1988, ApJ, 332, 96
- Lanzetta, K. M., Bowen, D. B., Tytler, D., and Webb, J. K. 1995, ApJ, 442, 538
- Lauroesch, J. T., Truran, J. W., Welty, D. E., and York, D. G. 1996, PASP, 108, 641
- Le Brun, V., Bergeron, J., Boissé, P., and Deharving, J. M. 1997, A&A, 321, 733
- Le Brun, V., Bergeron, J., Boissé, P. 1996, A&A, 306, 691
- Lilly, S. J., Tresse, L., Hammer, F., Crampton, D., and Le Fèvre, O. 1995, ApJ, 455, 108
- Linder, S. M. 1997, ApJ, in press
- McGaugh, S. 1994, ApJ, 426, 135
- Petitjean, P., and Bergeron, J. 1990, A&A, 231, 309 (PB90)
- Petitjean, P., Rauch, M., and Carswell, R. F. 1994, A&A, 291, 29
- Salpeter, E. E. 1993, AJ, 106, 1265
- Sargent, W. L. W., Boksenberg, A., and Steidel, C. C. 1988, ApJS, 68, 539
- Sargent, W. L. W., Steidel, C. C., and Boksenberg, A. 1988, ApJ, 334, 22 (SSB)
- Savage, B. D., and Sembach, K. R. 1996, ARAA, 34, 279
- Savage, B. D., and Sembach, K. R. 1991, ApJ, 379, 245
- Schechter, P. 1976, ApJ, 203, 297
- Schneider, D. P. et al. 1993, ApJS, 87, 45
- Sembach, K. R., and Savage, B. D. 1992, ApJS, 83, 147
- Steidel, C. C., Pettini, M., Dickinson, M., and Persson, S. E. 1994, AJ, 108, 2046
- Steidel, C. C. 1995, in ESO Workshop on Quasar Absorption Lines, ed. G. Meylan, (Garching : Springer-Verlag), 139
- Steidel, C. C. 1996, private communication
- Steidel, C. C., Dickinson, M., and Persson, S. E. 1994, ApJ, L75
- Steidel, C. C., and Sargent, W. L. W. 1992, ApJS, 80, 1 (SS92)
- Stengler-Larrea, E. A., et al. 1995, ApJ, 444, 64
- Thimm, G. 1995, in ESO Workshop on Quasar Absorption Lines, ed. G. Meylan, (Garching : Springer-Verlag), 169
- Tripp, T. M., Lu, L., and Savage, B. D. 1997, ApJS, 112, 1
- Tytler, D., Boksenberg, A., Sargent, W. L. W., Young, P., and Kunth, D. 1987, ApJS, 64, 667 (TBSYK)
- Uomoto, A. 1984, ApJ, 284, 497
- van Gorkom, J. H., Carilli, C. L., Stocke, J. T., Perlman, E. S., Shull, J. M. 1996, AJ, 112, 1397
- Vogt, S. S., et al. 1994, SPIE, 2198, 362
- Womble, D. 1995 Workshop on Quasar Absorption Lines, ed. G. Meylan, (Garching : Springer-Verlag), 158
- Yanny, B., and York, D. G. 1992, ApJ, 391, 569

This 2-column preprint was prepared with the AAS L^AT_EX macros v4.0.

TABLE 1
HIRES/KECK AND FOS/*HST* DATA

Object	z_{em}	HIRES Spectra			FOS Spectra	
		Date [UT]	Exp [s] ^a	λ Range [Å] ^b	Source	Grating
0002 + 051	1.899	1994 Jul 05	2700	3655.7 – 6079.0	KP	270H
0058 + 019	1.959	1996 Jul 18	3000	3766.2 – 5791.3
0117 + 212	1.491	1995 Jan 23	5400	4317.7 – 6775.1	KP	270H
0420 – 014	0.915	1995 Jan 23	3600	3810.5 – 6304.9
0450 – 132	2.253	1995 Jan 24	5400	3986.5 – 6424.5
0454 + 036	1.343	1995 Jan 22	4500	3765.8 – 6198.9	AR	270H
0454 – 220	0.534	1995 Jan 22	5400	3765.8 – 6198.9	AR	270H
0823 – 223	...	1995 Jan 24	3600	3977.8 – 6411.8	AR	270H
0958 + 551	1.755	1995 Jan 23	3600	5400.0 – 7830.0	KP	270H
1148 + 384	1.299	1995 Jan 24	5400	3986.5 – 6424.5
1206 + 456	1.155	1995 Jan 23	3600	3810.5 – 6304.9	KP	270H
1213 – 003	2.691	1995 Jan 24	5200	5008.1 – 7356.7
1222 + 228	2.040	1995 Jan 23	3600	3810.5 – 6304.9	AR	270H
1225 + 317	2.219	1995 Jan 24	2400	5737.5 – 8194.7
1241 + 174	1.282	1995 Jan 22	2400	3765.8 – 6189.9	KP	270H
1248 + 401	1.032	1995 Jan 22	4200	3765.8 – 6189.9	KP	270H
1254 + 044	1.018	1995 Jan 22	2400	3765.8 – 6189.9	KP	270H
1317 + 274	1.014	1995 Jan 23	3600	3810.5 – 6304.9	AR	270H
1329 + 412	1.937	1996 Jul 18	6300	3766.2 – 5791.3	AR	270H
1354 + 193	0.719	1995 Jan 22	3600	3765.8 – 6189.9	KP	270H
1421 + 331	1.906	1995 Jan 23	3600	3818.6 – 6316.9
1548 + 092	2.749	1996 Jul 19	3600	3766.2 – 5791.3
1622 + 235	0.927	1994 Jul 04	16200	3726.9 – 6191.0	AR	270H
		1994 Jul 05	3040			
1634 + 704	1.335	1994 Jul 04	2700	3723.3 – 6185.7	AR	270H
		1994 Jul 05	5400			
2128 – 123	0.501	1996 Jul 19	3900	3766.2 – 5791.3	KP	270H
2145 + 064	0.999	1996 Jul 18	4500	3766.2 – 5791.3	AR	270H

^aTotal exposure time is sum of combined frames.

^bAbove 5100 Å there are small gaps in the wavelength coverage.

NOTE.—“AR” denotes FOS spectrum taken from the *HST* archive and “KP” denotes FOS spectrum obtained from the Key Project.

TABLE 2
SAMPLE OF ABSORBERS

ID	z_{abs}	QSO	ω_v [km s ⁻¹]	$W_r(\lambda 2796)$ [Å]	DR	$Z(W_r, \text{DR})$
S1	0.456415	1421 + 331	6.45 ± 0.98	0.179 ± 0.019	1.15 ± 0.09	17.24
S2	0.500786	1329 + 412	25.57 ± 1.39	0.258 ± 0.035	1.33 ± 0.41	17.26
S3 ^a	0.521498	1354 + 193	6.57 ± 1.14	0.030 ± 0.007	1.31 ± 0.68	15.74
S4	0.550202	1222 + 228	9.58 ± 1.25	0.080 ± 0.014	1.30 ± 0.35	17.05
S5	0.558443	1241 + 174	17.17 ± 1.10	0.135 ± 0.014	2.03 ± 0.62	17.19
S6	0.591485	0002 + 051	4.96 ± 0.73	0.103 ± 0.008	1.62 ± 0.31	17.13
S7	0.642827	0454 + 039	4.77 ± 0.57	0.118 ± 0.008	1.46 ± 0.19	17.18
S8 ^a	0.705472	0823 - 223	11.86 ± 0.68	0.092 ± 0.007	2.09 ± 0.70	17.06
S9	0.725175	0058 + 019	9.30 ± 0.45	0.253 ± 0.012	1.26 ± 0.12	17.26
S10	0.729071	0117 + 212	47.4 ± 1.39	0.238 ± 0.009	1.71 ± 0.18	17.25
S11	0.770646	1548 + 092	9.53 ± 0.85	0.234 ± 0.024	1.19 ± 0.19	17.25
S12	0.818157	1634 + 706	3.14 ± 1.56	0.030 ± 0.018	1.68 ± 0.61	17.67
S13	0.843247	1421 + 331	3.08 ± 0.75	0.086 ± 0.008	1.01 ± 0.13	15.09
S14	0.854554	1248 + 401	62.68 ± 9.42	0.235 ± 0.014	1.76 ± 0.25	17.25
S15 ^a	0.866529	0002 + 051	1.68 ± 0.54	0.023 ± 0.008	1.62 ± 0.35	14.44
S16 ^a	0.895493	1241 + 174	4.95 ± 1.21	0.018 ± 0.005	1.87 ± 0.41	12.71
S17	0.905554	1634 + 706	4.07 ± 0.64	0.064 ± 0.004	1.42 ± 0.17	16.96
S18 ^a	0.931502	0454 + 039	4.36 ± 0.89	0.042 ± 0.005	1.84 ± 0.28	16.34
S19	0.934283	1206 + 459	7.67 ± 0.83	0.049 ± 0.005	2.02 ± 0.50	16.53
S20	0.956029	0002 + 051	6.24 ± 0.98	0.052 ± 0.007	2.07 ± 0.61	16.60
S21	0.973867	1329 + 412	26.79 ± 2.72	0.181 ± 0.035	1.41 ± 0.62	17.24
S22	0.998358	1329 + 412	6.72 ± 0.65	0.142 ± 0.010	1.51 ± 0.26	17.22
S23	1.041443	1634 + 706	17.19 ± 1.07	0.097 ± 0.008	2.10 ± 0.44	17.08
S24	1.127698	1213 - 003	4.17 ± 1.07	0.036 ± 0.006	1.86 ± 0.69	16.03
S25	1.211316	0958 + 551	3.43 ± 1.08	0.060 ± 0.007	1.36 ± 0.34	16.93
S26	1.229475	0450 - 132	10.00 ± 0.93	0.135 ± 0.010	1.29 ± 0.16	17.21
S27	1.232440	0450 - 132	22.72 ± 2.45	0.101 ± 0.009	1.44 ± 0.21	17.13
S28	1.272377	0958 + 051	4.86 ± 0.62	0.081 ± 0.007	1.45 ± 0.24	17.04
S29	1.325004	0117 + 212	76.09 ± 1.46	0.291 ± 0.011	1.60 ± 0.11	17.26
S30 ^b	1.342969	0117 + 212	44.95 ± 3.67	0.153 ± 0.008

^aQuantities obtained using Gaussian fitting to data.

^bThe $\lambda 2796$ transition was not covered. All quantities based upon $\lambda 2803$ transition.

TABLE 3
SYSTEM PROPERTIES

Ion/Tran	$\lambda_{\text{abs}}^{\text{a}}$ [Å]	EW_{r} [Å]
S1	Q1421 + 331	$z_{\text{abs}} = 0.45642$
Mg II 2796	4072.649	0.179 ± 0.019
Mg II 2803	4083.105	0.155 ± 0.020
Mg I 2853	4155.100	< 0.014
S2	Q1329 + 412	$z_{\text{abs}} = 0.50079$
Fe II 2587	3882.008	< 0.092
Fe II 2600	3902.303	< 0.100
Mg II 2796	4196.726	0.258 ± 0.035
Mg II 2803	4207.500	0.194 ± 0.054
Mg I 2853	4281.688	< 0.038
S3	Q1354 + 193	$z_{\text{abs}} = 0.52149$
Fe II 2587	3935.583	< 0.016
Fe II 2600	3956.158	< 0.012
Mg II 2796 ^b	4254.644	0.030 ± 0.007
Mg II 2803	4265.567	0.023 ± 0.010
Mg I 2853	4340.779	< 0.007
S4	Q1222 + 228	$z_{\text{abs}} = 0.55020$
Fe II 2587	4009.830	< 0.011
Fe II 2600	4030.793	< 0.009
Mg II 2796	4334.910	0.080 ± 0.014
Mg II 2803	4346.039	0.061 ± 0.013
Mg I 2853	4422.670	< 0.008
S5	Q1241 + 174	$z_{\text{abs}} = 0.55844$
Fe II 2587 ^c	4031.147	...
Fe II 2600	4052.221	< 0.012
Mg II 2796	4357.955	0.135 ± 0.014
Mg II 2803	4369.143	0.066 ± 0.019
Mg I 2853	4446.182	< 0.008

TABLE 3—*Continued*

Ion/Tran	$\lambda_{\text{abs}}^{\text{a}}$ [Å]	EW_r [Å]
S6	Q0002 + 051	$z_{\text{abs}} = 0.59149$
FeII 2344	3730.781	< 0.026
FeII 2374	3778.919	< 0.032
FeII 2383	3792.135	< 0.020
FeII 2587	4116.615	< 0.014
FeII 2600	4138.136	< 0.012
MgII 2796	4450.352	0.103 ± 0.008
MgII 2803	4461.778	0.064 ± 0.011
MgI 2853	4540.449	< 0.010
S7	Q0454 + 036	$z_{\text{abs}} = 0.64283$
FeII 2344	3851.138	< 0.031
FeII 2374	3900.829	< 0.019
FeII 2383	3914.471	0.029 ± 0.005
FeII 2587 ^d	4249.418	0.014 ± 0.004
FeII 2600	4271.634	0.037 ± 0.014
MgII 2796	4593.923	0.118 ± 0.008
MgII 2803	4605.716	0.081 ± 0.009
MgI 2853	4686.926	< 0.005
S8	Q0823 – 223	$z_{\text{abs}} = 0.70547$
FeII 2344	3997.991	< 0.019
FeII 2374	4049.577	< 0.016
FeII 2383	4063.739	< 0.017
FeII 2587	4411.459	< 0.008
FeII 2600	4434.522	< 0.008
MgII 2796	4769.100	0.092 ± 0.007
MgII 2803	4781.344	0.044 ± 0.011
MgI 2853	4865.650	< 0.005
S9	Q0058 + 019	$z_{\text{abs}} = 0.72518$
FeII 2344	4044.179	< 0.026
FeII 2374	4096.361	< 0.020
FeII 2383	4110.687	< 0.018
FeII 2587	4462.424	< 0.013
FeII 2600 ^d	4485.753	0.017 ± 0.005
MgII 2796	4824.197	0.253 ± 0.012
MgII 2803	4836.582	0.201 ± 0.016
MgI 2853	4921.862	0.041 ± 0.026

TABLE 3—*Continued*

Ion/Tran	$\lambda_{\text{abs}}^{\text{a}}$ [Å]	EW_r [Å]
S10	Q0117 + 212	$z_{\text{abs}} = 0.72907$
FeII 2587 ^d	4472.502	0.012 ± 0.002
FeII 2600	4495.884	0.075 ± 0.016
MgII 2796	4835.091	0.238 ± 0.009
MgII 2803	4847.504	0.132 ± 0.013
MgI 2853	4932.977	0.013 ± 0.009
S11	Q1548 + 093	$z_{\text{abs}} = 0.77065$
FeII 2374	4204.330	< 0.190
FeII 2383	4219.033	< 0.131
FeII 2587 ^d	4580.041	0.143 ± 0.006
FeII 2600	4603.986	0.101 ± 0.027
MgII 2796	4951.349	0.234 ± 0.024
MgII 2803	4964.061	0.197 ± 0.025
MgI 2853	5051.589	0.051 ± 0.059
S12	Q1634 + 706	$z_{\text{abs}} = 0.81816$
FeII 2344	4262.149	< 0.019
FeII 2374	4317.143	< 0.017
FeII 2383	4332.241	< 0.019
FeII 2587	4702.936	< 0.007
FeII 2600	4727.523	< 0.008
MgII 2796	5084.207	0.030 ± 0.005
MgII 2803	5097.260	0.018 ± 0.006
MgI 2853	5187.136	< 0.004
S13	Q1421 + 331	$z_{\text{abs}} = 0.84325$
FeII 2344	4320.965	0.041 ± 0.015
FeII 2374	4376.718	0.028 ± 0.018
FeII 2383	4392.024	0.068 ± 0.011
FeII 2587	4767.835	0.048 ± 0.009
FeII 2600	4792.761	0.071 ± 0.014
MgII 2796	5154.367	0.086 ± 0.008
MgII 2803	5167.600	0.085 ± 0.007
MgI 2853	5258.717	0.022 ± 0.009

TABLE 3—*Continued*

Ion/Tran	$\lambda_{\text{abs}}^{\text{a}}$ [Å]	EW_r [Å]
S14	Q1248 + 401	$z_{\text{abs}} = 0.85455$
FeII 2344	4347.471	0.024 ± 0.010
FeII 2374	4403.567	< 0.023
FeII 2383	4418.966	0.035 ± 0.010
FeII 2587	4797.082	0.010 ± 0.009
FeII 2600	4822.161	0.031 ± 0.007
MgII 2796	5185.986	0.253 ± 0.014
MgII 2803	5199.300	0.136 ± 0.017
MgI 2853	5290.976	< 0.019
S15	Q0002 + 051	$z_{\text{abs}} = 0.86653$
FeII 2344	4375.543	< 0.004
FeII 2374	4432.001	< 0.009
FeII 2383	4447.500	< 0.006
FeII 2587	4828.057	< 0.007
FeII 2600	4853.298	< 0.010
MgII 2796	5219.472	0.023 ± 0.008
MgII 2803	5232.872	0.014 ± 0.007
MgI 2853	5325.140	< 0.007
S16	Q1241 + 174	$z_{\text{abs}} = 0.89549$
FeII 2344	4443.441	< 0.006
FeII 2374	4500.775	< 0.006
FeII 2383	4516.514	< 0.005
FeII 2587	4902.977	< 0.005
FeII 2600	4928.610	< 0.005
MgII 2796	5300.466	0.018 ± 0.005
MgII 2803	5314.073	0.010 ± 0.005
MgI 2853	5407.773	< 0.004
S17	Q1634 + 706	$z_{\text{abs}} = 0.90555$
FeII 2344	4467.026	< 0.008
FeII 2374	4524.664	< 0.008
FeII 2383	4540.487	< 0.010
FeII 2587	4929.001	< 0.005
FeII 2600	4954.770	< 0.005
MgII 2796	5328.600	0.064 ± 0.004
MgII 2803	5342.280	0.045 ± 0.005
MgI 2853	5436.477	< 0.004

TABLE 3—*Continued*

Ion/Tran	$\lambda_{\text{abs}}^{\text{a}}$ [Å]	EW_r [Å]
S18	Q0454 + 036	$z_{\text{abs}} = 0.93150$
FeII 2344	4527.854	< 0.005
FeII 2374	4586.277	< 0.004
FeII 2383	4602.315	0.030 ± 0.008
FeII 2587	4996.120	< 0.004
FeII 2600 ^e	5022.239	...
MgII 2796	5401.159	0.043 ± 0.005
MgII 2803	5415.026	0.023 ± 0.005
MgI 2853	5510.506	< 0.005
S19	Q1206 + 456	$z_{\text{abs}} = 0.93428$
FeII 2344	4534.373	< 0.005
FeII 2374 ^c	4592.880	...
FeII 2383	4608.942	< 0.005
FeII 2587	5003.313	< 0.004
FeII 2600	5029.470	< 0.004
MgII 2796	5408.936	0.049 ± 0.005
MgII 2803	5422.822	0.024 ± 0.005
MgI 2853	5518.440	< 0.004
S20	Q0002 + 051	$z_{\text{abs}} = 0.95603$
FeII 2344	4585.351	< 0.005
FeII 2374	4644.515	< 0.007
FeII 2383	4660.757	< 0.009
FeII 2587	5059.562	< 0.008
FeII 2600	5086.014	< 0.005
MgII 2796	5469.746	0.052 ± 0.007
MgII 2803	5483.788	0.025 ± 0.007
MgI 2853	5580.480	< 0.005
S21	Q1329 + 412	$z_{\text{abs}} = 0.97387$
FeII 2344	4627.167	< 0.025
FeII 2374	4686.871	< 0.032
FeII 2383	4703.261	< 0.027
FeII 2587	5105.703	< 0.026
FeII 2600	5132.395	< 0.028
MgII 2796	5519.627	0.181 ± 0.035
MgII 2803	5533.797	0.128 ± 0.050
MgI 2853	5631.371	< 0.024

TABLE 3—*Continued*

Ion/Tran	$\lambda_{\text{abs}}^{\text{a}}$ [Å]	EW_r [Å]
S22	Q1329 + 412	$z_{\text{abs}} = 0.99836$
FeII 2344	4684.579	0.044 ± 0.016
FeII 2374	4745.024	< 0.011
FeII 2383	4761.617	0.061 ± 0.013
FeII 2587	5169.053	< 0.011
FeII 2600	5196.076	0.058 ± 0.017
MgII 2796	5588.112	0.142 ± 0.010
MgII 2803	5602.459	0.094 ± 0.015
S23	Q1634 + 706	$z_{\text{abs}} = 1.04144$
FeII 2344	4785.579	< 0.008
FeII 2374	4847.327	< 0.006
FeII 2383	4864.279	< 0.005
FeII 2600	5308.105	< 0.038
MgII 2796	5708.593	0.097 ± 0.008
MgII 2803	5723.249	0.046 ± 0.009
MgI 2853	5824.163	< 0.003
S24	Q1213 – 003	$z_{\text{abs}} = 1.12770$
FeII 2374	5052.136	< 0.007
FeII 2383	5069.804	< 0.014
FeII 2587	5503.610	< 0.008
FeII 2600	5532.383	< 0.010
MgII 2796	5949.793	0.036 ± 0.006
MgII 2803	5965.067	0.019 ± 0.006
MgI 2853	6070.246	< 0.005
S25	Q0958 + 551	$z_{\text{abs}} = 1.21132$
FeII 2587	5719.901	< 0.011
FeII 2600	5749.804	< 0.006
MgII 2796	6183.618	0.060 ± 0.007
MgII 2803	6199.493	0.044 ± 0.010
MgI 2853	6308.805	< 0.010

TABLE 3—*Continued*

Ion/Tran	$\lambda_{\text{abs}}^{\text{a}}$ [Å]	EW_{r} [Å]
S26	Q0450 – 132	$z_{\text{abs}} = 1.22948$
AlIII 1855	4135.017	0.042 ± 0.009
AlIII 1863	4153.092	0.010 ± 0.005
FeII 2344	5226.367	0.015 ± 0.014
FeII 2383	5312.315	0.037 ± 0.010
FeII 2587	5766.872	< 0.007
FeII 2600	5797.020	0.039 ± 0.017
MgII 2796	6234.397	0.135 ± 0.010
MgII 2803	6250.402	0.105 ± 0.010
MgI 2853	6360.612	< 0.007
S27	Q0450 – 132	$z_{\text{abs}} = 1.23244$
FeII 2344	5233.317	< 0.008
FeII 2374	5300.842	< 0.008
FeII 2383	5319.380	0.011 ± 0.007
FeII 2587 ^d	5774.541	0.008 ± 0.002
MgII 2796	6242.688	0.101 ± 0.009
MgII 2803	6258.715	0.070 ± 0.008
MgI 2853 ^d	6369.071	0.005 ± 0.002
S28	Q0958 + 551	$z_{\text{abs}} = 1.27238$
FeII 2374	5395.671	< 0.007
FeII 2383 ^d	5414.540	0.009 ± 0.002
FeII 2587	5877.844	< 0.007
FeII 2600 ^{d,f}	5908.573	0.017 ± 0.004
MgII 2796	6354.366	0.081 ± 0.007
MgII 2803	6370.679	0.056 ± 0.008
MgI 2853 ^d	6483.010	0.007 ± 0.002
S29	Q0117 + 212	$z_{\text{abs}} = 1.32500$
AlIII 1863	4331.013	0.0162 ± 0.004
FeII 2344 ^d	5450.307	0.006 ± 0.002
FeII 2374	5520.632	< 0.017
FeII 2383	5539.938	0.030 ± 0.010
FeII 2587	6013.972	0.010 ± 0.005
FeII 2600	6045.412	0.026 ± 0.009
MgII 2796	6501.530	0.291 ± 0.009
MgII 2803	6518.221	0.180 ± 0.011
MgI 2853 ^d	6633.153	0.005 ± 0.002

TABLE 3—*Continued*

Ion/Tran	$\lambda_{\text{abs}}^{\text{a}}$ [Å]	EW_{r} [Å]
S30	Q0117 + 212	$z_{\text{abs}} = 1.34297$
AlIII 1855	4345.600	0.031 ± 0.003
AlIII 1863	4364.461	0.022 ± 0.003
FeII 2344	5492.421	0.018 ± 0.005
FeII 2374	5563.289	< 0.014
FeII 2383	5582.745	0.029 ± 0.004
FeII 2587	6060.441	0.012 ± 0.005
MgII 2796	6501.530	...
MgII 2803	6568.586	0.153 ± 0.008
MgI 2853	6684.406	< 0.010

^aWhen multiple components are present, λ_{abs} is $\lambda_{\text{r}}(1 + z_{\text{abs}})$.

^bCompromised by bad pixel (see §3.1).

^cConfused by blending (see §3.1)

^dNot a 5σ detection, but at least a $> 3\sigma$ detection.

^eCompromised by pen mark on the CCD.

^fNot captured by the CCD.

TABLE 4
IONIZATION CONDITIONS^a

ID	N_c	$W_r(\lambda 2796)$ [Å]	$W_r(\lambda 2600)$ [Å]	$W_r(\lambda 1548)$ [Å]	IC ^b	Other Refs
S1	1	0.179 ± 0.019		
S2	1	0.258 ± 0.035	< 0.100	< 0.393		
S3	1	0.030 ± 0.007	< 0.012	< 0.247		1
S4 ^c	1	0.080 ± 0.014	< 0.009	< 0.645		2
S5 ^d	1	0.135 ± 0.014	< 0.012	0.175 ± 0.055	H?	1
S6	1	0.103 ± 0.008	< 0.012	< 0.145		1
S7	1	0.118 ± 0.008	0.037 ± 0.014	< 0.130	L	3
S8	1	0.092 ± 0.007	< 0.008	< 0.130		
S9	1	0.253 ± 0.012	0.017 ± 0.005	...	L?,M?	
S10	5	0.238 ± 0.009	0.075 ± 0.016	< 0.088	L	1
S11	1	0.234 ± 0.024	0.101 ± 0.027	...	L?,M?	
S12	1	0.030 ± 0.018	< 0.008	< 0.034	L?	4
S13	1	0.086 ± 0.008	0.071 ± 0.014	...	L?,M?	
S14	6	0.235 ± 0.014	0.031 ± 0.007	0.718 ± 0.600	M	1
S15	1	0.023 ± 0.008	< 0.010	< 0.110		1
S16	1	0.018 ± 0.005	< 0.005	< 0.093		1
S17	1	0.064 ± 0.004	< 0.005	0.169 ± 0.017	H	4,5
S18 ^e	1	0.042 ± 0.005	0.022 ± 0.008	< 0.111	L	3
S19	1	0.049 ± 0.005	< 0.004	0.204 ± 0.042	H	1,6
S20	1	0.052 ± 0.007	< 0.005	0.479 ± 0.040	H	1
S21 ^d	1	0.181 ± 0.035	< 0.028	< 0.389		
S22	1	0.142 ± 0.010	0.058 ± 0.017	< 0.119	L	
S23	1	0.097 ± 0.008	< 0.038	0.424 ± 0.018	H?	1,4,5
S24	1	0.036 ± 0.006	< 0.010	...		
S25	1	0.060 ± 0.007	< 0.006	...		
S26	2	0.135 ± 0.010	0.039 ± 0.017	...	L?,M?	
S27 ^e	2	0.101 ± 0.009	0.008 ± 0.007	...		
S28	1	0.081 ± 0.007	0.017 ± 0.004	0.440 ± 0.030	M	7
S29	6	0.291 ± 0.011	0.026 ± 0.009	0.890 ± 0.060	M	8
S30	4	0.153 ± 0.008	0.022 ± 0.004	0.670 ± 0.050	M	8

^aLimits are 3σ .

^b“L”, “H”, and “M” refer to “low”, “high”, and “multi-phase” ionization conditions. See text for definitions.

^cUnrestrictive limit due to complex blend in Ly α forest. Ambiguous case.

^dCIV λ 1548 transitions could be Ly α line.

^e $W_r(2600)$ scaled from measured $W_r(2383)$ by ratio of oscillator strengths.

REFERENCES.—(1) Jannuzi et al. 1998; (2) Impey et al. 1996; (3) Churchill & Le Brun 1998; (4) Bachall et al. 1996; (5) Bergeron et al. 1994; (6) Churchill & Charlton 1988; (7) Sargent, Boksenberg, & Steidel 1988; (8) Steidel & Sargent 1992